


Evidence for the involvement of lipid rafts localized at the ER-mitochondria associated membranes in autophagosome formation

Tina Garofalo, Paola Matarrese, Valeria Manganelli, Matteo Marconi, Antonella Tinari, Lucrezia Gambardella, Alberto Faggioni, Roberta Misasi, Maurizio Sorice & Walter Malorni



To cite this article: Tina Garofalo, Paola Matarrese, Valeria Manganelli, Matteo Marconi, Antonella Tinari, Lucrezia Gambardella, Alberto Faggioni, Roberta Misasi, Maurizio Sorice & Walter Malorni (2016): Evidence for the involvement of lipid rafts localized at the ER-mitochondria associated membranes in autophagosome formation, *Autophagy*, DOI: [10.1080/15548627.2016.1160971](https://doi.org/10.1080/15548627.2016.1160971)

To link to this article: <http://dx.doi.org/10.1080/15548627.2016.1160971>

 View supplementary material 

 Published online: 28 Apr 2016.

 Submit your article to this journal 

 View related articles 

 View Crossmark data 

RESEARCH PAPER

Evidence for the involvement of lipid rafts localized at the ER-mitochondria associated membranes in autophagosome formation

Tina Garofalo^{a,†}, Paola Matarrese^{b,c,†}, Valeria Manganelli^a, Matteo Marconi^b, Antonella Tinari^d, Lucrezia Gambardella^b, Alberto Faggioni^a, Roberta Misasi^a, Maurizio Sorice^{a,#}, and Walter Malorni^{b,e,#}

^aDepartment of Experimental Medicine, Sapienza University, Rome, Italy; ^bSection of Cell Aging and Degeneration, Department of Drug Research and Evaluation, Istituto Superiore di Sanita', Rome, Italy; ^cCenter of Metabolomics, Rome, Italy; ^dDepartment of Technology and Health, Istituto Superiore di Sanita', Rome, Italy; ^eIstituto San Raffaele Pisana, Rome, Italy

ABSTRACT

Mitochondria-associated membranes (MAMs) are subdomains of the endoplasmic reticulum (ER) that interact with mitochondria. This membrane scrambling between ER and mitochondria appears to play a critical role in the earliest steps of autophagy. Recently, lipid microdomains, i.e. lipid rafts, have been identified as further actors of the autophagic process. In the present work, a series of biochemical and molecular analyses has been carried out in human fibroblasts with the specific aim of characterizing lipid rafts in MAMs and to decipher their possible implication in the autophagosome formation. In fact, the presence of lipid microdomains in MAMs has been detected and, in these structures, a molecular interaction of the ganglioside GD3, a paradigmatic “brick” of lipid rafts, with core-initiator proteins of autophagy, such as AMBRA1 and WIPI1, was revealed. This association seems thus to take place in the early phases of autophagic process in which MAMs have been hypothesized to play a key role. The functional activity of GD3 was suggested by the experiments carried out by knocking down *ST8SIA1* gene expression, i.e., the synthase that leads to the ganglioside formation. This experimental condition results in fact in the impairment of the ER-mitochondria crosstalk and the subsequent hindering of autophagosome nucleation. We thus hypothesize that MAM raft-like microdomains could be pivotal in the initial organelle scrambling activity that finally leads to the formation of autophagosome.

ARTICLE HISTORY

Received 15 July 2015
Revised 23 February 2016
Accepted 26 February 2016

KEYWORDS

AMBRA1; autophagosome; autophagy; calnexin; lipid rafts; mitochondria-associated membranes

Introduction

The interaction of the endoplasmic reticulum (ER) with mitochondria occurs via certain subdomains of the ER, named mitochondria-associated membranes (MAMs), which allow membrane “scrambling” between these organelles and contributes to the complex series of ER functions.^{1–3} Indeed, several regions of close apposition between the ER and mitochondria were detected by studies carried out several years ago.^{4,5} However, since these studies provided only ultrastructural observations, these reports remained neglected for a long time. In particular, while morphological evidence of the physical juxtaposition between ER and mitochondria was described since 1959,⁶ it was experimentally proven only 30 y later. In fact, analyzing ER fractions copurified with mitochondria in velocity sedimentation assays, mainly from rat liver cells, it was observed that mitochondria can tightly be associated with elements of the ER and that the communication and intermixing between ER and mitochondria can be mediated by MAMs.^{7–12} These works also showed that these cosedimenting fractions were enriched in enzymes responsible for the synthesis of lipids. These findings suggested that MAMs could act as sites

of nonvesicular lipid transfer between the ER and the mitochondria.¹³ It was thus hypothesized that there was a combined role of proteins and lipids, specifically cholesterol and glycosphingolipids (GSLs), in enabling the formation of MAMs and their physiological function(s).¹⁴


Cholesterol, a central constituent of biological membranes, plays a role in regulating a plethora of cellular processes, including gene transcription and signal transduction, and is particularly abundant in MAMs.¹⁵ Together with glycosphingolipids, it tends to cluster and form microdomains, named lipid rafts, which are dynamic assemblages of sphingolipids, cholesterol and proteins that dissociate and associate rapidly and form functional clusters¹⁶ detectable at cell membranes, including membranes of internal organelles, such as mitochondria and ER.^{17,18} These clusters provide highly efficient lipid-protein complexes, which operate in membrane trafficking and cell signaling. For instance, it has recently been reported that GM1, a “prototypic” ganglioside, which contains one sialic acid residue, can accumulate at the ER membranes and can promote the juxtaposition of ER and mitochondria at the MAMs.¹⁹ These findings underscored the possibility that “cooperation”

CONTACT Walter Malorni ✉ malorni@iss.it Department of Drug Research and Evaluation, Istituto Superiore di Sanita', viale Regina Elena 299, Rome 00161, Italy

Color versions of one or more of the figures in the article can be found online at www.tandfonline.com/kaup.

[†] To be considered as first investigators

[#] To be considered as senior investigators

 Supplemental data for this article can be accessed on the publisher's website.

© 2016 Taylor & Francis Group, LLC

could take place between lipids and proteins in regulating physiological scrambling pathways at membrane contact sites. In fact, microdomains have been hypothesized to contribute either to cell death, including apoptosis, or, of relevance here, to autophagy.^{20,21}

As concerns this latter (macroautophagy), this process represents a basic catabolic mechanism for intracellular degradation and recycling of unnecessary or dysfunctional cellular components and organelles that, through the action of lysosomes, can finally provide significant energy resources to the cell. During this process, cytoplasmic constituents are included within a double-membrane vesicle known as an autophagosome that fuses with a lysosome and forms the autolysosome.^{22–27} The autophagosome can originate from the plasma membrane, early endosomes, ER, and Golgi but, more recently, it has also been suggested that, at least in mammalian cells, autophagosomes could form at the ER–mitochondria contact sites, i.e. at MAMs.²⁸ In fact, after autophagic stimulation, the phagophore/omegasome (autophagosome precursor) marker ATG14 (autophagy-related 14) relocates at the ER–mitochondria contact sites. Moreover, key molecules involved in autophagosome formation, such as BECN1 and PIK3C3/Vps34 (phosphatidylinositol 3-kinase catalytic subunit type 3; the mammalian ortholog of yeast Vps34), have been hypothesized to be recruited at MAMs in cells under autophagic stimulation.²⁸ The first, BECN1 is a well known regulator of autophagy forming a complex with the class III phosphatidylinositol 3-kinase (PtdIns3K)²⁹ to generate phosphatidylinositol 3-phosphate (PtdIns3P), whereas PIK3C3 is a kinase whose activity is enhanced when AMBRA1 (autophagy/Beclin 1 regulator 1), a recently discovered autophagy-associated interactor, binds BECN1.^{30,31} In addition, PtdIns3P recruits effectors, such as WIPI1 (WD repeat protein, phosphoinositide interacting 1), to mediate the vesicle nucleation and autophagosome formation. Further actors appear however pivotal in the morphogenetic vesicle remodeling and reshaping associated with the autophagic cascade. In fact, we have recently analyzed the possible functional role for these molecules, mainly gangliosides, in the initiation phase of autophagosome biogenesis, demonstrating a strict molecular interaction between GD3, an acidic glycosphingolipid, and PtdIns3P.²¹ In particular, GD3 ganglioside, interacting with cytoskeletal network,^{32,33} can rapidly redistribute from the plasma membrane to the cell cytoplasm,^{34,35} including endosomal compartments, MAMs³⁶ and mitochondria;³⁷ and it can molecularly associate with MAP1LC3/LC3 (microtubule associated protein 1 light chain 3; a mammalian ortholog subfamily of yeast Atg8, whose nonsoluble form stably associates with phagophore membranes) early after autophagic initiation. Moreover, the inhibition of ceramide synthase as well as of GD3 synthase significantly hindered autophagosome formation, suggesting that gangliosides could contribute to autophagosome assembly.

In the present work, in light of the elegant work recently published by Hamasaki et al.,²⁸ we analyzed the possible implication of MAM lipid “rafts” in autophagosome formation. We found a molecular association of CANX (calnexin), a chaperone lectin involved in protein folding and quality control at the ER and a key molecular marker of MAMs,³⁸ with WIPI1 and AMBRA1, 2 important actors of autophagic flux.^{31,39,40}

Importantly, this association seems to occur in MAM lipid microdomains during the early phases of the autophagic process.

Results

Autophagy induction in primary human fibroblasts

We first characterized the autophagic process in our cell model. As shown in Fig. 1A, autophagy induced by amino acid starvation (Hank’s balanced salt solution, HBSS) was checked by: (i) flow cytometry by using a Cyto-ID Autophagy Detection kit, (ii) immunofluorescence by using an anti-LC3 antibody, and (iii) western blot analysis, using an anti-LC3 and an anti-phosphorylated (P-) ULK1 (unc-51 like autophagy activating kinase 1) antibody. We found a significant ($P < 0.01$) increase of green fluorescence after staining with a Cyto-ID Autophagy Detection kit in fibroblasts treated with HBSS for 1 h (upper left panel), and an evident increase of LC3 puncta, indicative of autophagic vesicles positivity, was also observed by fluorescence microscopy analysis in starved fibroblasts (micrographs). This increase of LC3 puncta was also quantified by morphometric analysis (upper right panel). Accordingly, western blot analysis revealed a band corresponding to LC3-II after cell starvation together with a significant decrease of P-ULK1 (bottom left panel). These results were also confirmed by densitometric analyses (bottom right panels, bar graphs).

Autophagy induction bolsters the presence of lipid rafts in MAMs

In order to figure out whether autophagy could involve a remodeling of MAMs and whether a participation of lipid rafts in this process could be revealed, we first characterized MAM-associated rafts during autophagy induced by HBSS.

Because MAMs have a higher concentration of cholesterol and a different phospholipid fatty acid composition as compared to the surrounding ER membrane,¹⁵ we investigated whether CANX, a prototypical Ca^{2+} -binding ER palmitoylated chaperone protein enriched in the MAMs, could be enriched in the detergent TX-100 insoluble fractions corresponding to lipid rafts. As shown in Fig. 1B, the analysis of the distribution of CANX was carried out in fractions obtained by a 5–30% linear sucrose gradient. These analyses revealed that this protein was mostly enriched in fraction 6 (specifically corresponding to raft-like microdomains) and fraction 7. These are possibly TX-100-resistant microdomains of a different composition. Under metabolic impairment conditions, i.e., after autophagic stimulation by amino acid starvation (HBSS), CANX was highly concentrated in fractions 4 to 6 (raft fraction), as also shown by densitometric analyses (right panel). As a control, we also analyzed the distribution of VDAC1 (voltage dependent anion channel 1), which is constitutively included in lipid rafts. In fact, VDAC1 was highly enriched in fractions 4 to 6 in both control and HBSS-treated cells (Fig. 1B, bottom). These results were also quantified by densitometric analyses (Fig. 1B, bottom right panel).

Based on our previous observations suggesting that the ganglioside GD3 can actively contribute to the biogenesis and

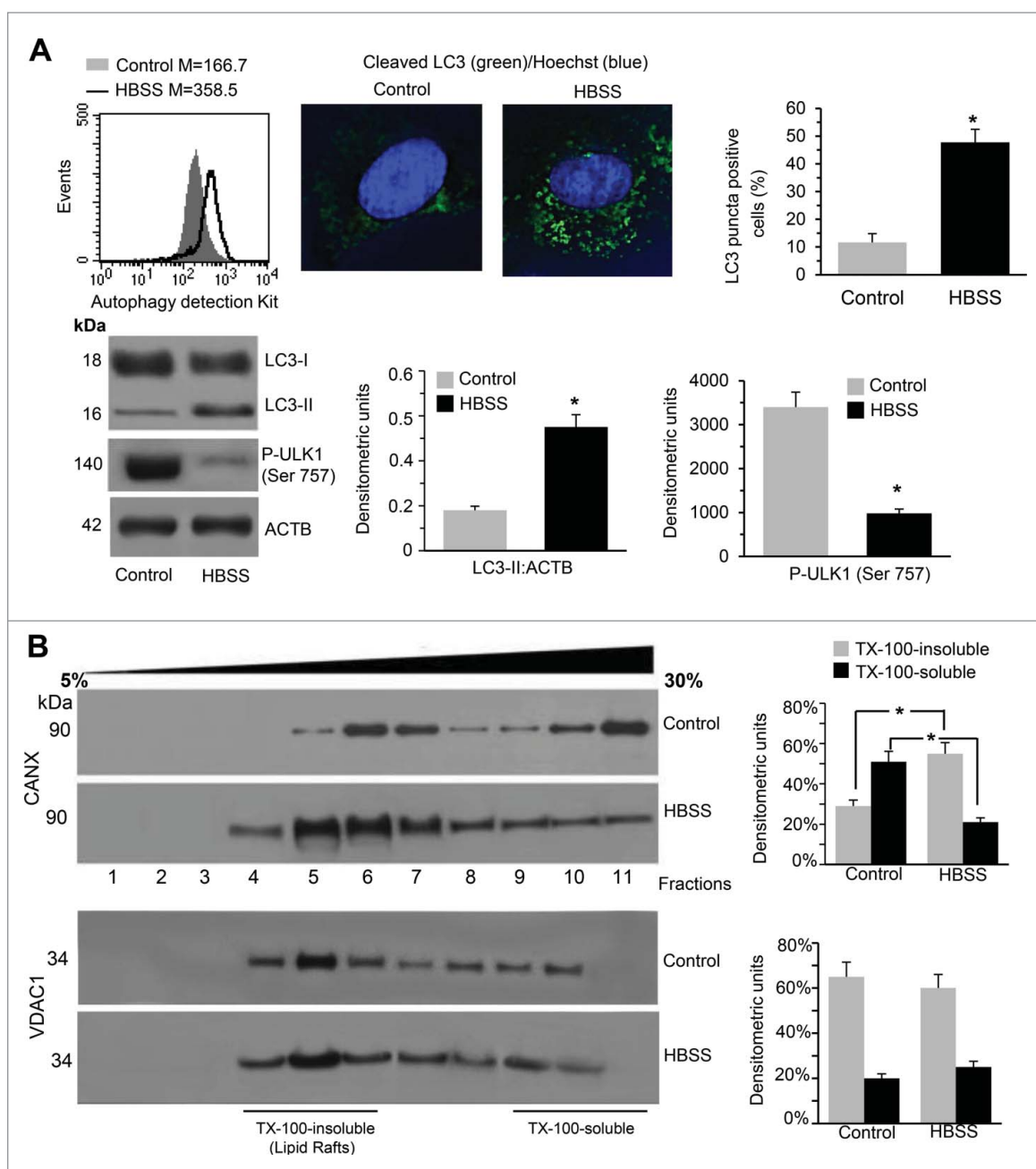


Figure 1. Autophagy induction bolsters the presence of lipid rafts in MAMs. (A) *Upper left panel.* Semiquantitative flow cytometry analysis of autophagy performed in primary human fibroblasts untreated (full gray curves) or starved 1 h with HBSS medium (empty curves) performed with a Cyto-ID Autophagy Detection kit. Numbers represent the median fluorescence intensity. A representative experiment among 3 is shown. *Upper middle pictures.* IVM analysis after LC3-Hoechst double staining of control cells (left picture) and of cells treated with HBSS for 1 h (right picture). *Upper right panel.* Bar graph shows the percentage of LC3 puncta-positive cells. *Bottom left panel.* Primary fibroblasts, untreated or treated with HBSS for 1 h at 37°C, were lysed in lysis buffer, subjected to 15% SDS-PAGE and analyzed by western blot using anti-LC3 PAb or anti-P-ULK1 (Ser757) PAb. Loading control was evaluated using anti-ACTB mAb. A representative experiment among 3 is shown. *Bottom, right panels.* Bar graphs show densitometric analysis. Results represent the mean \pm SD from 3 independent experiments. *, $P < 0.01$ HBSS vs control cells. (B) *Left panel.* Representative immunoblots of sucrose gradient fractions. Human fibroblast cells, either untreated or treated with HBSS for 1 h at 37°C, were lysed and the supernatant fraction was subject to sucrose density gradient. After centrifugation, the gradient was fractionated and each gradient fraction was recovered and analyzed by western blot analysis using an anti-CANX PAb. As control, fractions obtained after sucrose density gradient from untreated or treated cells were analyzed using an anti-VDAC1 PAb. *Right panel.* Densitometric analysis of sucrose gradient fractions. The columns indicate the percent distribution across the gel of raft fractions 4 to 6 (Triton X-100-insoluble fractions) and 9 to 11 (Triton X-100-soluble fractions), as detected by densitometric scanning analysis. Results represent the mean \pm SD from 3 independent experiments. *, TX-100-insoluble fractions from HBSS-treated cells vs TX-100-insoluble from control cells: $P < 0.01$; *, TX-100-soluble fractions from HBSS-treated cells vs TX-100-soluble from control cells: $P < 0.01$.

maturation of autophagic vacuoles,²¹ we evaluated by transmission electron microscopy the presence of MAMs in our autophagy (HBSS)-stimulated fibroblasts. Several adjacent structures corresponding to typical close contacts between the cisternae of rough endoplasmic reticulum and mitochondria were detected in stimulated cells only (compare Fig. 2A with Fig. 2B). In these

cells, several small vesicles in close proximity of mitochondria were also detected (Fig. 2C). A morphometric analysis carried out as stated in Materials and methods clearly indicated that in HBSS-treated cells these features were significantly more frequent than in fed cells (Table 1). Immunoelectron microscopy analysis was then carried out aimed at evaluating the possible

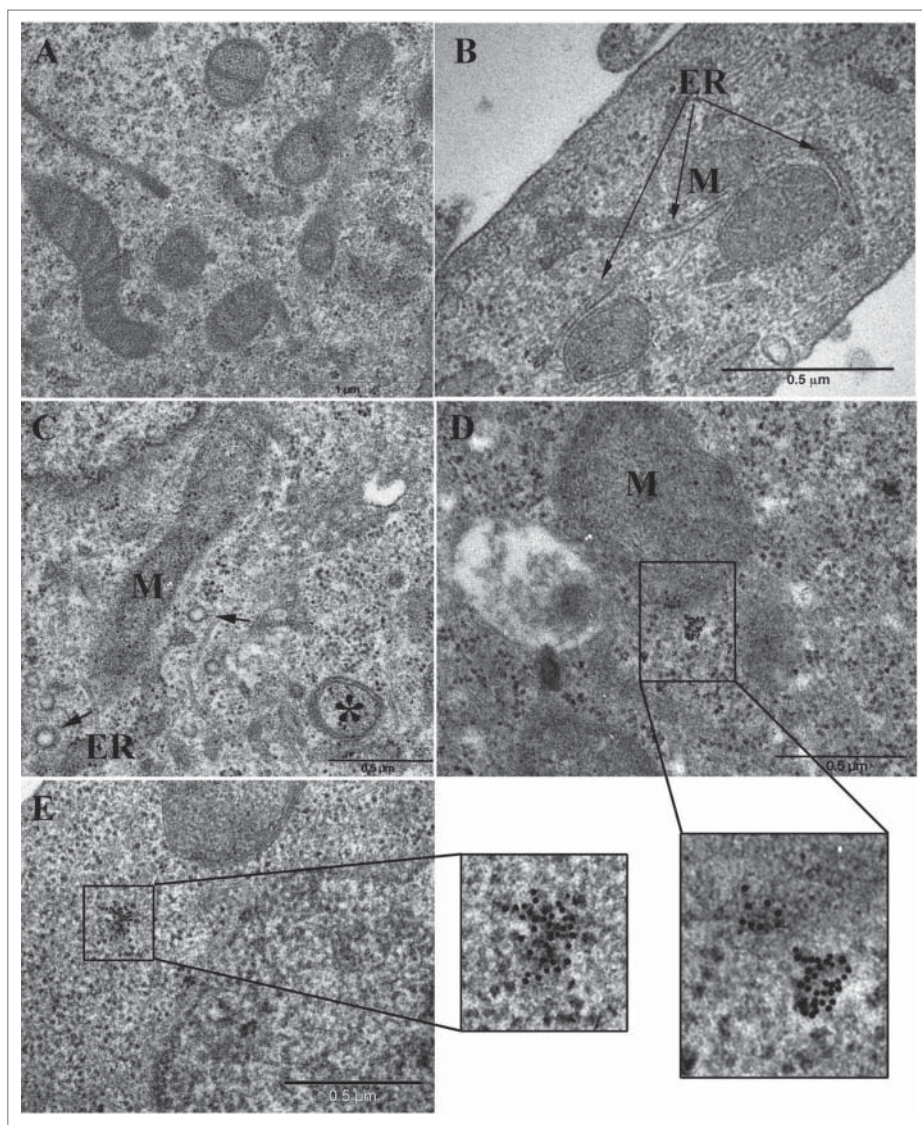


Figure 2. Autophagy induction and the presence of lipid rafts in MAMs. Transmission electron microscopy analysis of control and autophagy-stimulated cells. (A) Normal ER and mitochondria are observed in control cells while (B) ER cisternae (ER) and mitochondria (M) are detectable very close to each other in autophagy-induced cells. Moreover, (C) several small vesicles morphologically characterized by an electron-translucent core, probably MAMs next to mitochondria and to ER cisternae, can also be detected in autophagy-induced cells (arrows). Asterisk indicates a double-membrane autophagic vacuole. (D) Labeling of GD3 in these cells appears to be localized in these small vesicles in close proximity to mitochondria and at mitochondrial membrane as well (see enlarged area), whereas (E) in control cells GD3 gold labeling is often visible as a cluster of particles in the cell cytoplasm (see enlarged area).

presence of GD3 in small vesicles. The results obtained strongly suggested that ganglioside GD3, considered as a paradigmatic ganglioside component of raft-like microdomains,⁴¹ was detectable in MAMs of cells under autophagic stimulation (Fig. 2D, see enlarged area, and Table 1), being GD3 immunogold labeling negligible in normally fed cells (Fig. 2E, see enlarged area, and Table 1).³⁴

Ganglioside GD3 participates in the early events of the autophagic process

Under autophagic stimulation CANX associates with the ganglioside GD3. We investigated, by coimmunoprecipitation experiments, the possible interaction of CANX with the ganglioside GD3, considered as a paradigmatic constituent of microdomains, as suggested above. Dot-blot analysis, using a highly

Table 1. Morphometric analysis by transmission electron microscopy in fed and HBSS-treated cells.

	Fed		HBSS	
Localization	total	GD3 labeled	total	GD3 labeled
ER adjacent to mitochondria	18 (9%)	3 (17%)	86 (43%)	42 (49%)
Vesicles adjacent to mitochondria	6 (3%)	2 (33%)	68 (34%)	38 (56%)

Note. Number of cells displaying cisternae of the endoplasmic reticulum adjacent to mitochondria and vesicles adjacent to mitochondria, together with corresponding percentages, are indicated. GD3 gold labeling was also evaluated by analyzing either fed or HBSS-treated cells. The number of cells displaying gold particles (and the relative percentage) was very low in fed cells whereas, under starvation (HBSS), a significant percentage of cells showed gold particles on ER membranes close to the mitochondria as well as on vesicles close to the mitochondria. This seems to indicate a recruitment of ganglioside GD3 in MAMs under autophagic stimulation.

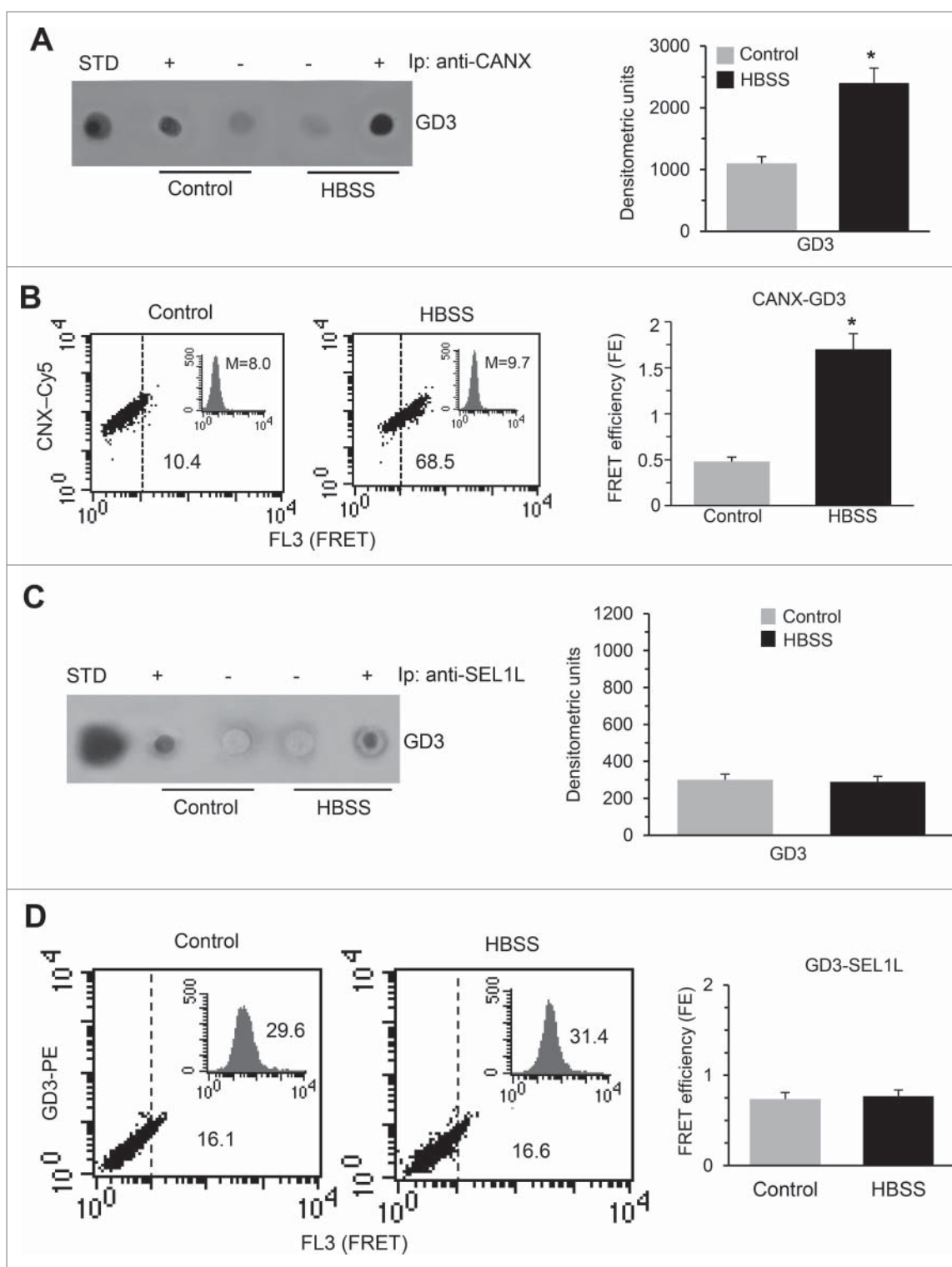


Figure 3. Under autophagic stimulation CANX associates with ganglioside GD3. (A) Primary human fibroblasts untreated or treated with HBSS for 1 h, were lysed in lysis buffer, followed by immunoprecipitation with rabbit anti-CANX PAb. A rabbit IgG isotypic control was employed. The immunoprecipitates were spotted onto nitrocellulose strips and incubated with R24 anti-GD3 MAb, as described in Materials and methods. A representative experiment among 3 is shown. Bar graph in the right panel shows densitometric analysis. Results represent the mean \pm SD from 3 independent experiments. *, $P < 0.01$ HBSS vs Control cells. (B) Flow cytometry analysis of GD3-CANX association by FRET technique in: control cells (left panel) and in cells treated with HBSS 1 h (middle panel). Numbers indicate the percentage of FL3-positive events obtained in one experiment representative of 3. Inserts represent GD3 intracellular amount in the corresponding sample and was quantitatively expressed by the median fluorescence intensity. Bar graph (right panel) shows evaluation of FE, according to the Riemann algorithm, of GD3-CANX association. Results represent the mean \pm SD from 3 independent experiments. *, $P < 0.01$ HBSS vs Control cells. (C) Primary human fibroblasts untreated or treated with HBSS for 1 h, were lysed in lysis buffer, followed by immunoprecipitation with rabbit anti-SEL1L PAb. A rabbit IgG isotypic control was employed. The immunoprecipitates were spotted onto nitrocellulose strips and incubated with R24 anti-GD3 MAb, as described in Materials and methods. A representative experiment among 3 is shown. Bar graph in the right panel shows densitometric analysis. Results represent the mean \pm SD from 3 independent experiments. (D) Quantitative FRET analysis of GD3-SEL1L association in control cells (left panel) and in HBSS-treated fibroblasts (middle panel). Numbers indicate the percentage of FL3-positive events obtained in one experiment representative of 3. Inserts represent SEL1L intracellular amount in the corresponding sample and was quantitatively expressed by the median fluorescence intensity. Bar graph shows evaluation of FE, according to the Riemann algorithm. Results represent the mean \pm SD from 3 independent experiments. No statistically significant differences were found between Control and HBSS-treated samples.

specific anti-GD3 monoclonal antibody (MAb), and densitometric analysis of CANX immunoprecipitates revealed that in unstimulated control cells GD3 was weakly associated with CANX, but, after autophagic triggering by HBSS, the association of GD3 with CANX was significantly increased (Fig. 3A, densitometric analysis in the right panel).

These results, obtained by using biochemical methods, were also confirmed by using the FRET technique (Fig. 3B). This last approach, whose sensitivity allows performing a quantitative analysis by using significantly smaller amounts of biological material than immunoprecipitation techniques, revealed a weak interaction between CANX and GD3 in unstimulated cells that significantly increased after HBSS treatment. This was further demonstrated by FRET efficiency (FE) calculation performed by pooling together the results obtained from 3 independent experiments (Fig. 3B, bar graph).

To verify if this interaction was specific to CANX and it was not due to changes in the ER membrane composition under starvation conditions, we performed parallel coimmunoprecipitation experiments in order to analyze the association of GD3 with SEL1L (SEL1L ERAD E3 ligase adaptor subunit) molecule, an ER-associated adaptor protein with the same overall topology of CANX.⁴² Dot blot and densitometric analysis of SEL1L immunoprecipitates showed that GD3 was weakly associated with SEL1L either in untreated or in HBSS-treated cells (Fig. 3C). These results, were also confirmed by using FRET technique (Fig. 3D). In fact, calculation of FE by the Riemann algorithm clearly showed a moderate, although statistically significant ($P < 0.01$ vs negative control), molecular association between SEL1L and GD3 but, importantly, this association was not influenced by autophagy induction. That is, no statistically significant differences were observed between control and HBSS-treated cells (Fig. 3D, bar graph).

Under autophagic stimulation CANX associates with AMBRA1 and WIPI1. Coimmunoprecipitation experiments were then carried out in order to assess the possible interaction of CANX with crucial upstream regulators of autophagy enabling autophagosome nucleation, i.e. with the entire AMBRA1-PtdIns 3 kinase complex, including WIPI1, PIK3C3, BECN1 (Beclin 1, autophagy related) ATG14 and UVRAG (UV radiation resistance associated). AMBRA1 is a BECN1-interacting protein that positively regulates the BECN1-dependent program of autophagy.^{30,31} WIPI1 is an essential PtdIns3P effector protein involved in autophagosome formation at the omegasome.^{39,40}

Cell lysates were immunoprecipitated with anti-CANX polyclonal antibody (PAb), followed by protein G-acrylic beads. Results of western blot and densitometric analyses, shown in Fig. 4A, revealed a positive band of coimmunoprecipitation corresponding to AMBRA1, which was more evident in cells stimulated with HBSS. Similar findings were found analyzing the association of CANX with WIPI1 in the same immunoprecipitates. In fact, western blot analysis showed that, in control cells, WIPI1 was weakly associated with CANX whereas, after treatment with HBSS, a proportion of WIPI1 was associated with CANX (Fig. 4A). In addition, PIK3C3, BECN1, ATG14 and UVRAG were detectable in CANX immunoprecipitates after HBSS treatment only. Virtually, no bands were detected in control immunoprecipitation

experiments carried out with an IgG having irrelevant specificity (Fig. 4A).

Recent data suggest a direct binding between ATG16L1 (autophagy-related 16 like 1) and WIPI2,⁴³ 2 important autophagy-related proteins acting downstream of the AMBRA1-BECN1 complex. Hence, we investigated whether these proteins could be recruited to the CANX-GD3 complex after autophagy induction. Western blot analysis showed that ATG16L1 and WIPI2 were not detectable in CANX immunoprecipitates (Fig. 4A), either in untreated or HBSS-treated cell extracts, suggesting that these molecules do not interact with CANX. As a purity control, i.e., in order to exclude microsomes derived from the ER in our preparations, the samples were analyzed for the presence of POR (P450 [cytochrome] oxidoreductase), a specific microsomal marker.⁴⁴ However, this marker was virtually absent in our preparations (Fig. 4A). Again, FRET analysis confirmed the results obtained by biochemical methods (Fig. 4B). As a further control, in parallel experiments, cell lysates from HBSS-treated and untreated cells were immunoprecipitated with anti-SEL1L PAb, followed by protein G-acrylic beads. The immunoprecipitates were then subjected to western blot analysis. No bands corresponding to AMBRA1, WIPI1, ATG16L1, or WIPI2 were detected (Fig. S1).

Under autophagic stimulation GD3 associates with AMBRA1 and WIPI1. On the basis of the above reported results we investigated the possible interaction of GD3 with AMBRA1. Therefore, AMBRA1 immunoprecipitates were subjected to dot blot analysis using an anti-GD3 mAb. The analysis revealed that, while in control unstimulated cells GD3 was only weakly associated with AMBRA1, after triggering with HBSS, the association of GD3 with AMBRA1 was significantly increased (Fig. 5A, densitometric analysis in the right panel). These data were also confirmed by quantitative FRET analysis (Fig. 5B). In the same immunoprecipitates the possible interaction of AMBRA1 with CANX was also investigated. Western blot analysis (Fig. 5C), showed a positive band of coimmunoprecipitation, which was more evident in cells stimulated with HBSS, indicating an increased interaction of these molecules (AMBRA1 and CANX) after autophagy induction. In addition, we also evaluated the association of AMBRA1 with WIPI1. Results of western blot analysis showed that, while in unstimulated control cells WIPI1 was slightly associated with AMBRA1, after triggering with HBSS a proportion of WIPI1 was found associated with AMBRA1. We then investigated the possible recruitment of ATG16L1 and WIPI2 to the AMBRA1-GD3 complex after autophagic triggering. Western blot analysis showed that ATG16L1 and WIPI2 were virtually undetectable in AMBRA1 immunoprecipitates either from untreated or HBSS-treated cells (Fig. 5C). No bands were detected in control immunoprecipitation experiments with an IgG having irrelevant specificity (Fig. 5C). As far as WIPI family proteins was concerned, FRET analysis revealed that WIPI1 was strongly associated with AMBRA1 after HBSS treatment (Fig. 5D, upper panels), whereas WIPI2 was not (Fig. 5D, bottom panels), thus confirming results obtained by biochemical methods. All in all, these experiments suggested that, under autophagic stimulation, a molecular interaction between ganglioside GD3, AMBRA1 and WIPI1 with the MAM marker CANX clearly occurs.

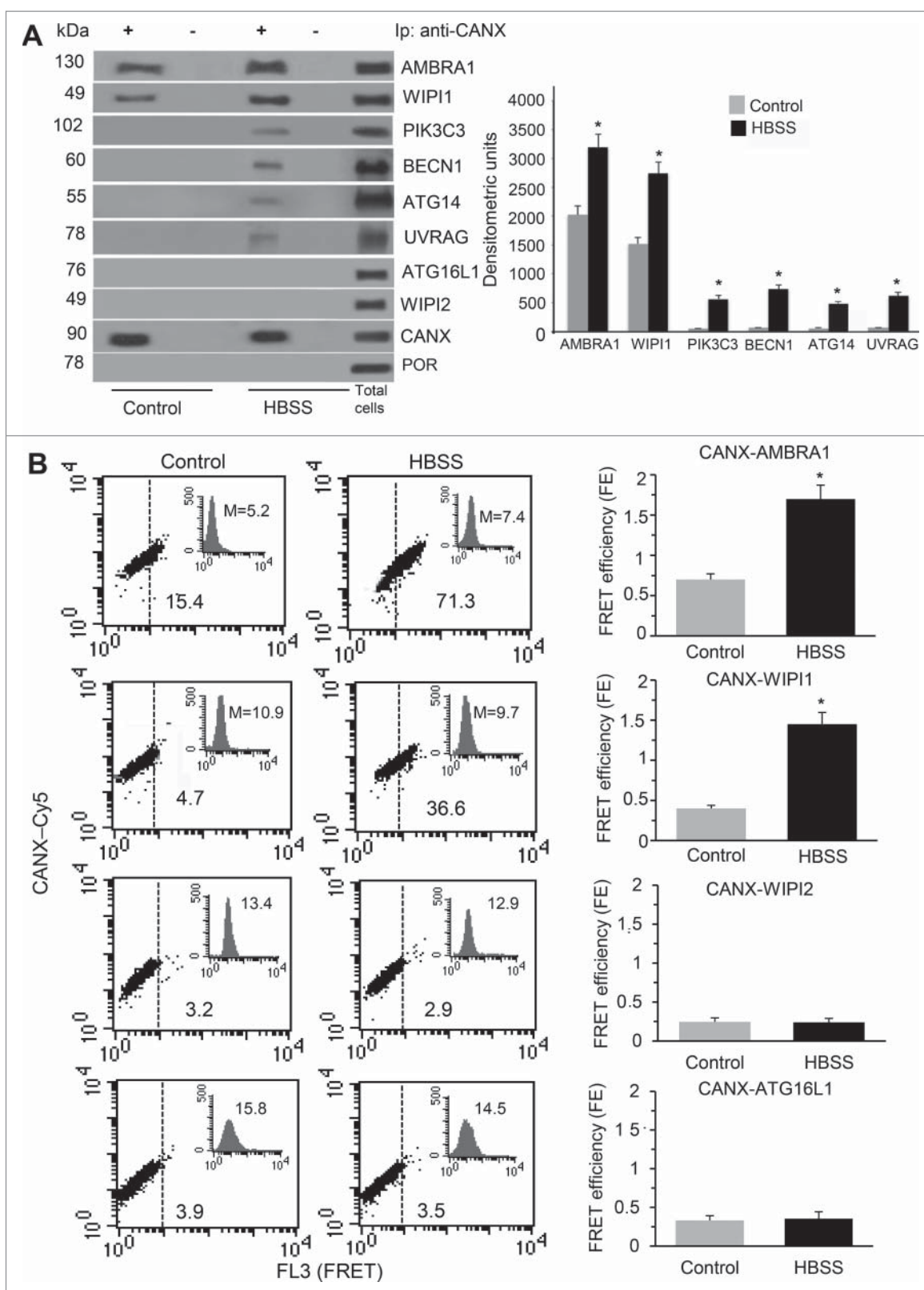


Figure 4. CANX associates with AMBRA1 and WIPI1 under autophagic stimulation. (A) Coimmunoprecipitation of CANX with AMBRA1, WIPI1, ATG16L1 and WIPI2 in control cells and in cells treated with HBSS for 1 h. Primary fibroblasts, untreated or treated with HBSS, were lysed in lysis buffer, followed by immunoprecipitation with rabbit anti-CANX PAb. A rabbit IgG isotypic control was employed. The immunoprecipitates were analyzed for the presence of AMBRA1 by western blot analysis, using anti-AMBRA1 PAb. In parallel, the immunoprecipitates were checked for the presence of WIPI1, PIK3C3, BECN1, ATG14, UVRAG, ATG16L1 and WIPI2 by western blot analysis, using the anti-WIPI1 MAb, anti-PIK3C3, anti-BECN1, anti-ATG14, anti-UVRAG, anti-ATG16L1 and anti-WIPI2 PAbs. A representative experiment among 3 is shown. As a control, the immunoprecipitates were assessed by immunoblot with anti-CANX MAb or anti-POR PAb. Bar graph in the right panel shows densitometric analysis. Results represent the mean \pm SD from 3 independent experiments. *, $P < 0.01$ HBSS vs control cells. (B) Flow cytometry analysis of CANX-AMBRA1, CANX-WIPI1, CANX-WIPI2 and CANX-ATG16L1 association by FRET technique in: control cells (left panels) and in cells treated with HBSS 1 h (middle panels). Numbers indicate the percentage of FL3-positive events obtained in one experiment representative of 3. Inserts represent AMBRA1, WIPI1, WIPI2 and ATG16L1 intracellular amount, respectively, in the corresponding sample quantitatively expressed as median fluorescence intensity. Bar graphs (right panels) show evaluation of FE, according to the Riemann algorithm. Results represent the mean \pm SD from 3 independent experiments. *, $P < 0.01$ HBSS vs control cells.

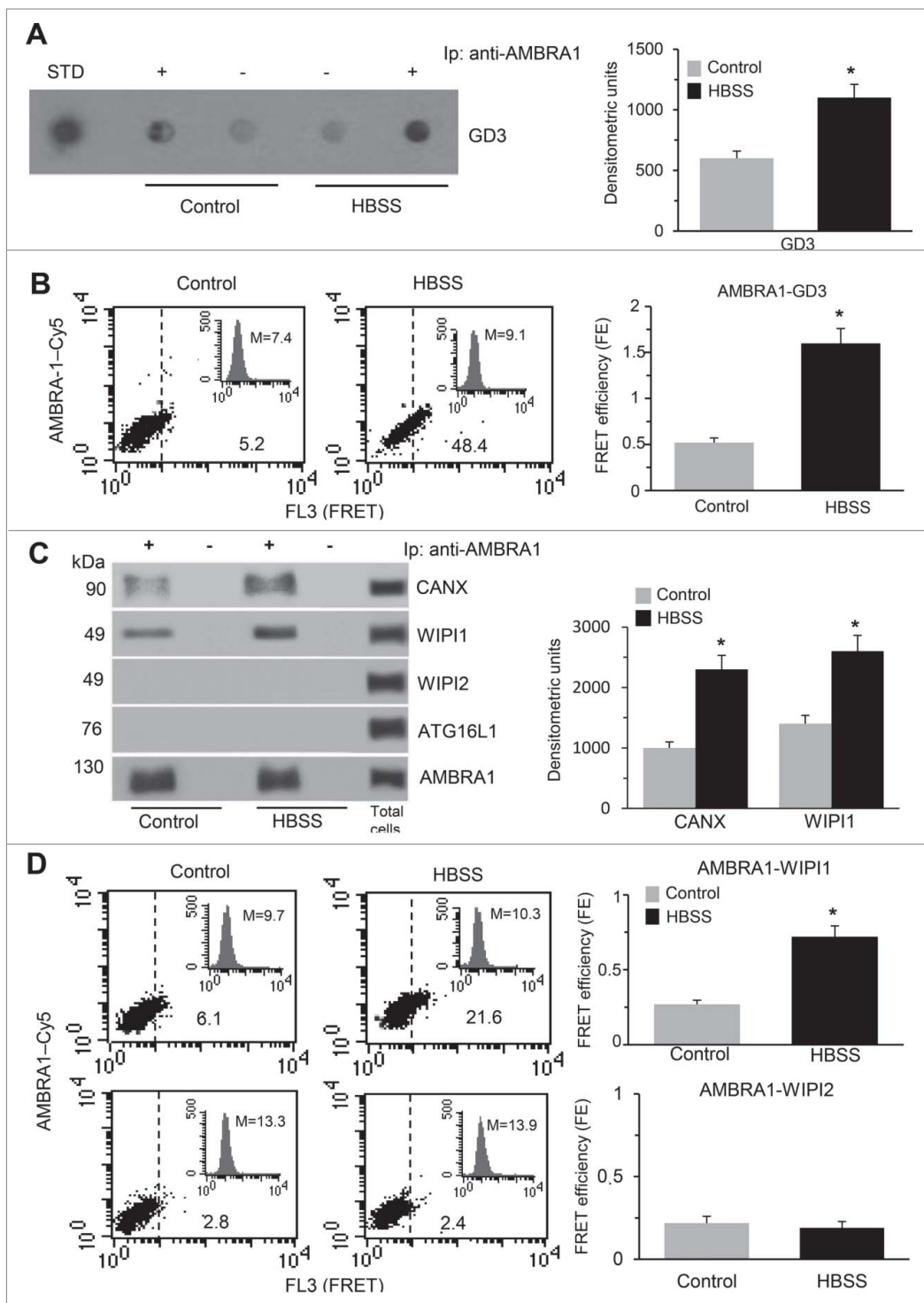


Figure 5. Ganglioside GD3 participates in the early events of the autophagic process. (A) Primary human fibroblasts untreated or treated with HBSS for 1 h, were lysed in lysis buffer, followed by immunoprecipitation with rabbit anti-AMBRA1 PAb. A rabbit IgG isotypic control was employed. The immunoprecipitates were spotted onto nitrocellulose strips and incubated with R24 anti-GD3 mAb, as described in Materials and methods. A representative experiment among 3 is shown. Bar graph in the right panel shows densitometric analysis. Results represent the mean \pm SD from 3 independent experiments. *, $P < 0.01$ HBSS vs control cells. (B) Flow cytometry analysis of GD3-AMBRA1 association by FRET technique in: control cells (left panel) and in cells treated with HBSS 1 h (middle panel). Numbers indicate the percentage of FL3-positive events obtained in one experiment representative of 3. Inserts represent GD3 intracellular amount in the corresponding sample and was quantitatively expressed by the median fluorescence intensity. Bar graph (right panel) shows evaluation of FE, according to the Riemann algorithm, of GD3-AMBRA1 association. Results represent the mean \pm SD from 3 independent experiments. (C) Coimmunoprecipitation of AMBRA1 with CANX, WIPI1, WIPI2 and ATG16L1 in control cells and in cells treated with HBSS for 1 h. Primary fibroblasts, untreated or treated with HBSS, were lysed in lysis buffer, followed by immunoprecipitation with rabbit anti-AMBRA1 PAb. A rabbit IgG isotypic control was employed. The immunoprecipitates were analyzed for the presence of CANX by western blot analysis, using anti-CANX PAb. In parallel, the immunoprecipitates were checked for the presence of WIPI1, WIPI2 and ATG16L1 by western blot analysis, using anti-WIPI1 MAb, anti-WIPI2 PAb and anti-ATG16L1 PAb. A representative experiment among 3 is shown. As a control, the immunoprecipitates were assessed by immunoblot with anti-AMBRA1 MAb. Bar graph in the right panel shows densitometric analysis. Results represent the mean \pm SD from 3 independent experiments. (D) Flow cytometry analysis of AMBRA1-WIPI1 and AMBRA1-WIPI2 association by FRET technique in: control cells (left panel) and in cells treated with HBSS for 1 h (middle panel). Numbers indicate the percentage of FL3-positive events obtained in one experiment representative of 3. Inserts represent WIPI1 and WIPI2 intracellular amount in the corresponding sample quantitatively expressed by the median fluorescence intensity. Bar graph shows evaluation of FE, according to the Riemann algorithm, of AMBRA1-WIPI1 and AMBRA1-WIPI2 association. Results represent the mean \pm SD from 3 independent experiments. *, $P < 0.01$ HBSS vs control cells.

Involvement of MAMs in early events of autophagosome formation: experiments in isolated MAMs

In order to better analyze MAM components, isolated MAM fractions were then considered. In particular, we analyzed the implication of lipid rafts and the possible presence of key molecules involved in the early events of autophagic flux in isolated MAMs. Since AMBRA1, BECN1 and PIK3C3 have been defined as the autophagy core complex, which plays a key role in the early events of the autophagic process,^{30,31,45} and on the basis of the above results, we checked isolated MAMs for the presence of the autophagy-related interactors BECN1 and PIK3C3, whose recruitment to MAMs after autophagic stimulation has recently been reported.²⁸ According to this work,²⁸ we preliminarily confirmed that these molecules were increased in MAMs isolated from starved cells (data not shown). Then, analyzing isolated MAMs for the presence of AMBRA1 and WIPI1, we found that: (i) a consistent amount of AMBRA1 and a small amount of WIPI1 were constitutively present in MAM fractions but, also, that (ii) under starvation conditions the presence of these proteins in the MAM fractions was significantly increased (Fig. 6A, left panel, bar graph on the right panel indicates densitometric analysis). In line with the results reported above, ATG16L1 and WIPI2 were virtually absent in the isolated MAM fractions (Fig. 6A).

The purity of the same MAM preparations was checked by analyzing CANX and VDAC1, 2 proteins known to be enriched in these membranes, TOMM20 (translocase of outer mitochondrial membrane 20 homolog [yeast]), a typical mitochondrial marker absent in MAMs, as well as P4HB (prolyl 4-hydroxylase subunit β), an ER-associated protein marker (Fig. 6B). We found that CANX and VDAC1 were detected in MAMs either isolated from control or from HBSS-treated cells (Fig. 6B, left panel). As expected, in pure mitochondrial fractions only VDAC1 and TOMM20 were detectable, independently from any treatment (Fig. 6B, right panel). Moreover, since a strict molecular interaction has previously been shown between GD3 and PtdIns3P suggesting a role for GD3 in the omegasome formation,²¹ we decided to assess by dot blot analysis using a highly specific anti-GD3 MAb, the possible presence of GD3 in the same isolated MAM fractions considered above. We found that, in line with transmission electron microscopy (TEM) observations (Fig. 2), the association of GD3 with MAMs was well evident after autophagy induction, i.e. after cell starvation with HBSS (Fig. 6C, left panel, bar graph on the right indicates densitometric analysis).

Knocking down ST8SIA1 expression impairs CANX-AMBRA1 association at the MAM level hindering autophagy

In order to clarify the role of GD3 during autophagic process, a small interfering RNA (siRNA) was employed to knock down *ST8SIA1* (*ST8* α -N-acetyl-neuraminidase α -2,8-sialyltransferase 1) gene expression, a member of the glycosyltransferase family responsible for the synthesis of GD3. Under our experimental conditions, we found that 48 h after siRNA addition: (i) more than 65% of cells were transfected (Fig. 7A, upper left panel, positive control siGLO *LMNA* [*lamin A/C*] siRNA-FITC) and

that (ii) in cells transfected with *ST8SIA1* siRNA a significant reduction (about 70%) of *ST8SIA1*, with respect to scrambled siRNA-transfected cells, was detectable (Fig. 7A, upper middle panel). In addition, as previously reported,²¹ flow cytometry analyses of *ST8SIA1* siRNA-treated cells, incubated with HBSS as above and stained with a Cyto-ID Autophagy Detection kit, revealed that autophagy was significantly reduced as compared to scrambled siRNA-transfected cells (Fig. 7A, upper right panel). As a further control, we also knocked down *ATG5* (autophagy-related 5) gene expression under the same experimental conditions. As expected, we found that transfection with *ATG5* siRNA (Fig. 7A, bottom left panel) significantly reduced expression level of the *ATG5* protein (Fig. 7A, bottom middle panel). Consequently, autophagy induced by HBSS, as revealed after cell staining with a Cyto-ID Autophagy Detection kit, was significantly impaired in *ATG5* siRNA-transfected cells, in comparison with scrambled siRNA-transfected cells (Fig. 7A, bottom right panel).

Moreover, autophagy inhibition in *ST8SIA1*-downregulated cells was also verified by: (i) immunofluorescence, by using an anti-LC3 antibody, and (ii) western blot analysis, using an anti-LC3 antibody (Fig. 7B). As expected, the LC3 puncta formation (Fig. 7B, micrographs, upper left panel) and the increase of the band corresponding to LC3-II (Fig. 7B, bottom left panel) induced by HBSS were significantly reduced in cells transfected with siRNA for *ST8SIA1* in comparison to scrambled siRNA-transfected cells. These results were also confirmed by morphometric and densitometric analyses (Fig. 7B, right panels, bar graphs).

Importantly, FRET analysis revealed that in fibroblasts transfected with *ST8SIA1* siRNA, HBSS did not induce any increase of CANX-AMBRA1 association (Fig. 7C, middle panel) and CANX-BECN1 association (not shown) that, at variance, were detectable in HBSS-treated, scrambled siRNA-transfected cells (Fig. 7C, left panel). In fact, statistical analysis, performed after the application of the Riemann algorithm, revealed that the association CANX-AMBRA1 (expressed as FE) in *ST8SIA1* siRNA-transfected cells was significantly lower than in scrambled siRNA-transfected cells after autophagic triggering by HBSS (Fig. 7C, right panel). Thus, the protein composition of MAMs seems to be altered by the knocking down of GD3 ganglioside so that the starvation-induced association of core complex molecules at the MAMs was impaired.

Knocking down MFN2 gene expression reduces HBSS-induced autophagy and CANX-AMBRA1 association

It has been reported that MAMs are enriched in MFN2 (mitofusin 2).⁴⁶ Since MFN2 also localizes at the ER where, via its interaction with mitochondrial mitofusins, is responsible of inter-organelle bridges formation, we decided to investigate the role of this GTPase in our experimental system by using a small interfering RNA (siRNA). Forty-eight h after *MFN2* siRNA transfection we observed that: (i) about 70% of cells were transfected (Fig. 8A, upper left panel, positive control *GFP-22* siRNA) and that (ii) cells transfected with *MFN2* siRNA showed a significant reduction in the expression level of this protein, in comparison to control siRNA-transfected cells (Fig. 8A, upper middle panel). Interestingly, we also observed

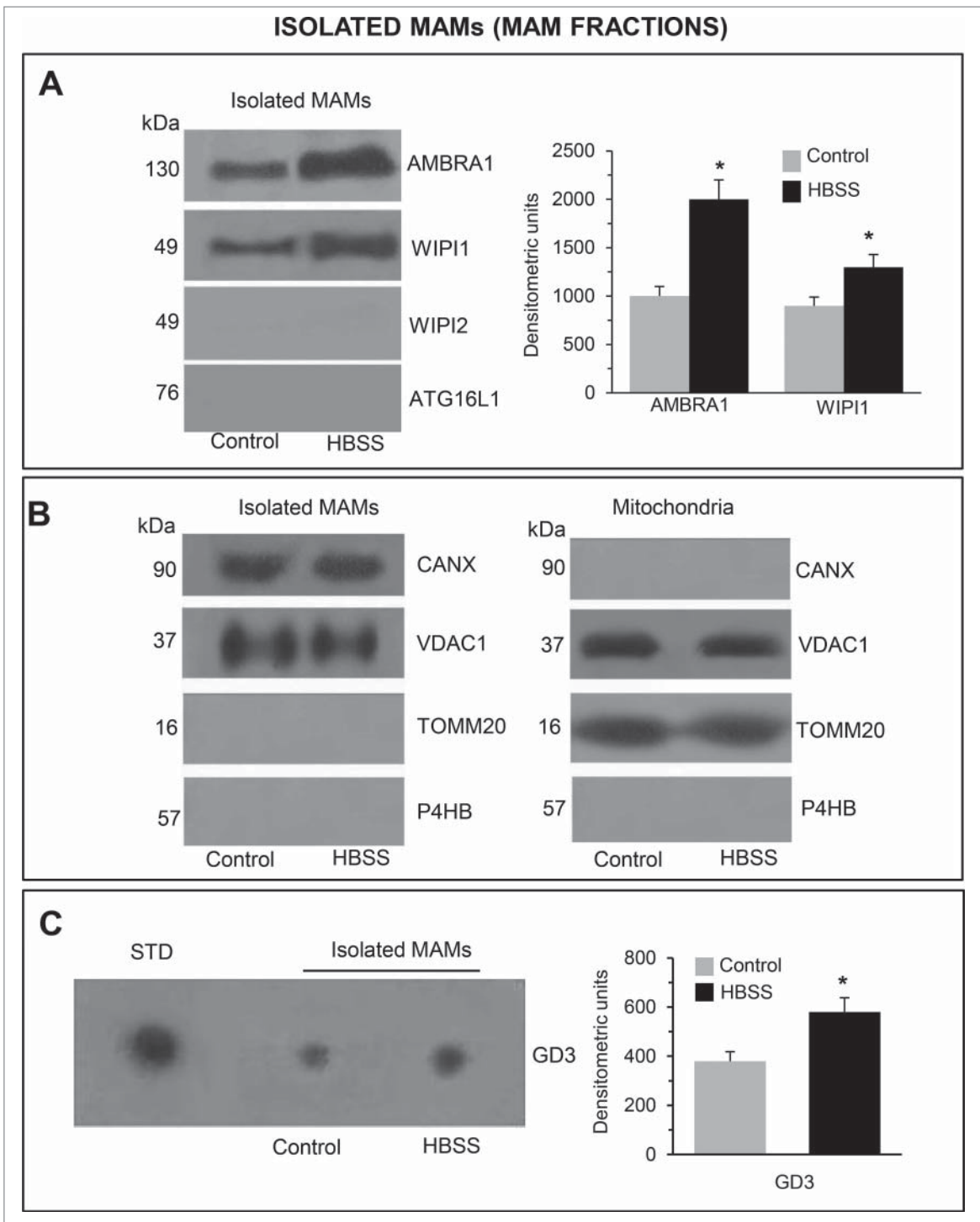


Figure 6. Involvement of MAMs in early events of autophagosome formation: experiments in isolated MAMs. Pure mitochondria preparations obtained from fibroblast cells, either untreated or treated with HBSS for 1 h, were subjected to Percoll gradient fractionation. After centrifugation, high-purity MAM fractions were obtained. (A) Isolated MAMs were analyzed by western blot using an anti-AMBRA1 mAb, anti-WIPI1 PAb, anti-WIPI2 PAb and anti-ATG16L1 PAb. A representative experiment among 3 is shown. Bar graph in the right panel shows densitometric analysis. Results represent the mean \pm SD from 3 independent experiments. (B) Isolated MAMs, as well as pure mitochondria fractions, were checked for MAM purity by western blot, using antibodies vs mitochondrial marker TOMM20, MAM markers CANX and VDAC1 and ER marker P4HB. (C) Isolated MAMs were analyzed by Dot blot. Samples were spotted onto nitrocellulose strips and incubated with anti-GD3 R24 MAb, as described in Materials and methods. A positive control was obtained using pure standard GD3 (STD). A representative experiment among 3 is shown. Bar graph in the right panel shows densitometric analysis. *, $P < 0.01$ HBSS vs control cells.

that when *MFN2* siRNA-transfected cells were incubated for 1 h with HBSS, the autophagy induction was significantly reduced in comparison with HBSS-treated cells transfected with control siRNA, as revealed with a Cyto-ID Autophagy Detection kit (Fig. 8A, upper right panel). These observations

were also confirmed by immunofluorescence and western blot analysis, performed by using an anti-LC3 antibody (Fig. 8B). In fact, according to flow cytometry data, we found that LC3 puncta induced by HBSS treatment were significantly reduced by *MFN2* knockdown (Fig. 8B, micrographs, upper left panel).

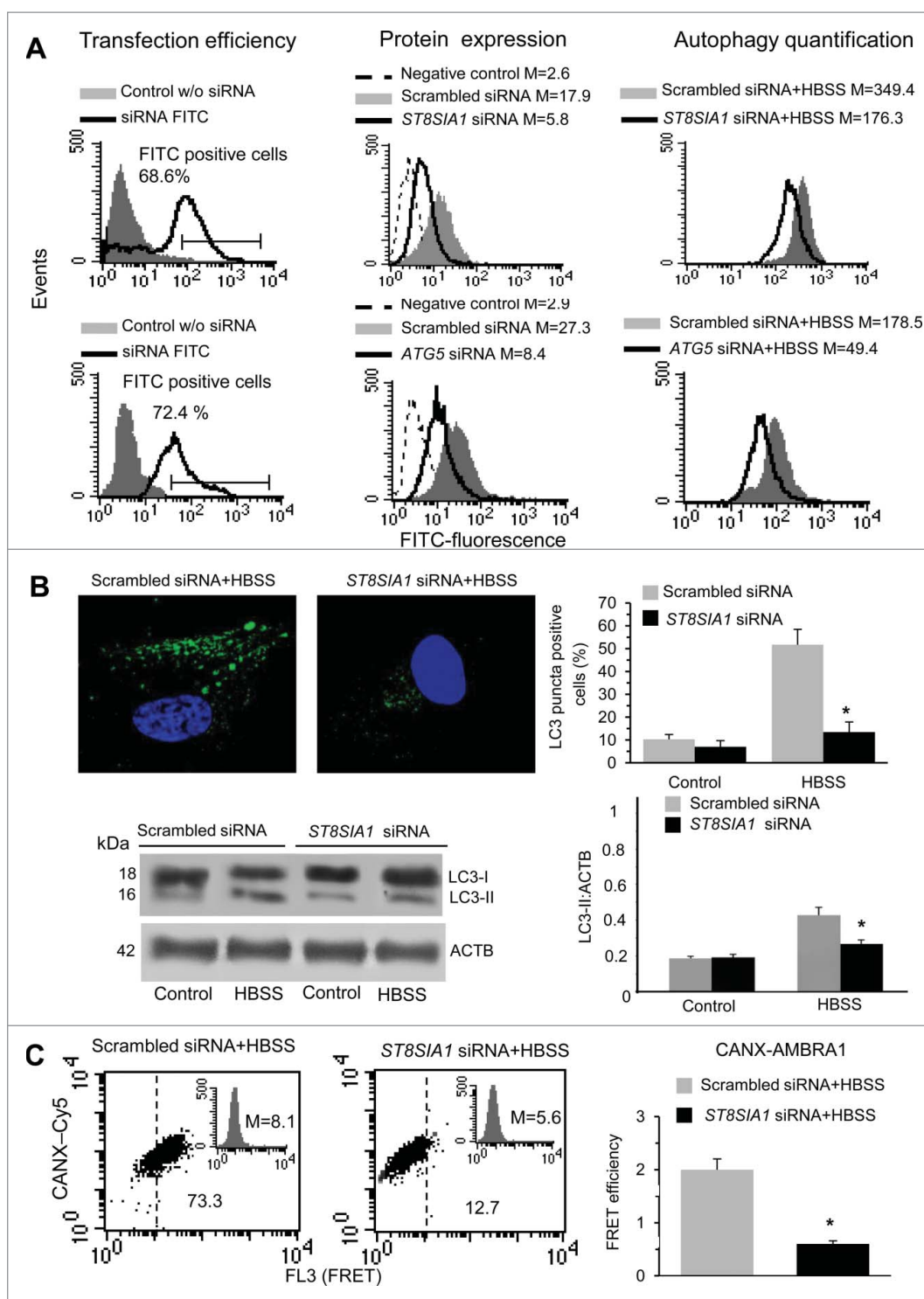


Figure 7. Knocking down *ST8SIA1* gene (GD3 synthase) expression impairs CANX-AMBRA1 association at the MAM level hindering autophagy. (A) *Upper left panel.* Cytofluorimetric analysis of fluorescence emission in fibroblasts transfected with FITC-siRNA. The percentage of FITC-positive cells was considered indicative of the transfection efficiency. *Upper middle panel.* Cytofluorimetric evaluation of *ST8SIA1* expression level 48 h after specific siRNA transfection. *Upper right panel.* Semiquantitative flow cytometry analysis performed with a Cyto-ID Autophagy detection kit of autophagy induced by HBSS in fibroblasts knocked down for *ST8SIA1* or in cells transfected with scrambled siRNA. *Bottom left panel.* Cytofluorimetric analysis of fluorescence emission in fibroblasts transfected with FITC-siRNA. The percentage of FITC-positive cells was considered indicative of the transfection efficiency. *Bottom middle panel.* Cytofluorimetric evaluation of *ATG5* expression level 48 h after specific siRNA transfection. *Bottom right panel.* Semiquantitative flow cytometry analysis performed with a Cyto-ID Autophagy detection kit of autophagy induced by HBSS in fibroblasts knocked down for *ATG5* or in cells transfected with scrambled siRNA. In the left panels, the number represents the mean percentage \pm SD of FITC-positive cells (corresponding to transfected cells) obtained in 3 independent measurements. In the middle panels, the numbers represent the mean \pm SD of the median fluorescence intensity obtained in 3 independent experiments. A representative experiment is shown. (B) *Upper panels.* IVM analysis after LC3-Hoechst double staining of cells knocked down for *ST8SIA1* and treated with HBSS for 1 h and of cells transfected with scrambled siRNA and treated with HBSS for 1 h. Bar graph on the right shows the percentage of LC3 puncta-positive cells. *Bottom panels.* Western blot analysis using an anti-LC3 PAb. Loading control was evaluated using anti-ACTB Mab. A representative experiment among 3 is shown. Bar graph to the right shows densitometric analysis. Results represent the mean \pm SD from 3 independent experiments. In HBSS samples ^{***} indicates $P < 0.01$ between *ST8SIA1* siRNA and scrambled siRNA. (C) FRET analysis of CANX-AMBRA1 in fibroblasts knocked down for *ST8SIA1* and treated with HBSS for 1 h (middle panel) or in cells transfected with scrambled siRNA and treated with HBSS for 1 h (left panel). Numbers indicate the percentage of FL3-positive events obtained in one experiment representative of 3. Inserts represent AMBRA1 intracellular amount in the corresponding sample and was quantitatively expressed by the median fluorescence intensity. Bar graph shows the evaluation of FE, according to the Riemann algorithm. Results represent the mean \pm SD from 3 independent experiments. *, $P < 0.01$ vs scrambled siRNA.

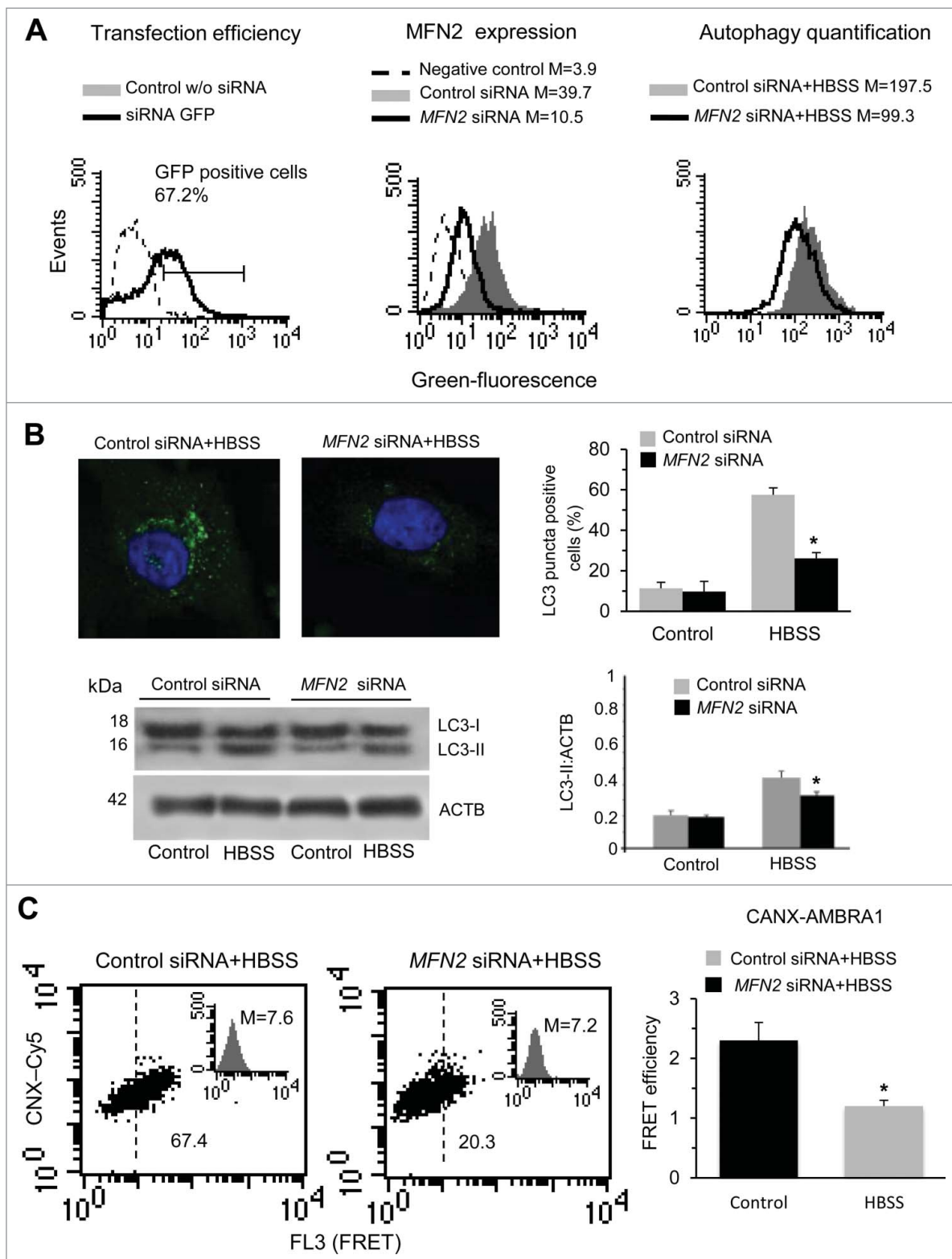


Figure 8. Knocking down *MFN2* gene expression reduces HBSS-induced autophagy and CANX-AMBRA1 association. (A) *Upper left panel.* Cytofluorimetric analysis of fluorescence emission in fibroblasts transfected with *GFP-22* siRNA. The percentage of GFP-positive cells was considered as indicative of the transfection efficiency. *Upper middle panel.* Cytofluorimetric evaluation of *MFN2* expression level 48 h after specific siRNA transfection. *Upper right panel.* Semiquantitative flow cytometry analysis performed with a Cyto-ID Autophagy Detection kit of autophagy induced by HBSS in fibroblasts knocked down for *MFN2* as well as in cells transfected with control siRNA. In the left panels, the number represents the mean percentage \pm SD of GFP-positive cells (corresponding to transfected cells) obtained in 3 independent experiments. In the middle panel, the numbers represent the mean \pm SD of the median fluorescence intensity obtained in 3 independent experiments. A representative experiment is shown. (B) *Upper panels.* IVM analysis after LC3-Hoechst double staining of cells knocked down for *MFN2* or transfected with control siRNA and then treated with HBSS for 1 h. Bar graph on the right shows the percentage of LC3 puncta-positive cells. *Bottom panels.* Western blot analysis using an anti-LC3 Pab. Loading control was evaluated using anti-ACTB mAb. A representative experiment among 3 is shown. Bar graph to the right shows densitometric analysis. Results represent the mean \pm SD from 3 independent experiments. ^{***} indicates $P < 0.01$ between *MFN2* siRNA and control siRNA after HBSS treatment. (C) FRET analysis of CANX-AMBRA1 in fibroblasts knocked down for *MFN2* and treated with HBSS for 1 h (middle panel) or in cells transfected with control siRNA and treated with HBSS for 1 h (left panel). Numbers indicate the percentage of FL3-positive events obtained in one experiment representative of 3. Inserts represent AMBRA1 intracellular amount in the corresponding sample and was quantitatively expressed by the median fluorescence intensity. Bar graph on the right shows the evaluation of FE, according to the Riemann algorithm. Results represent the mean \pm SD from 3 independent experiments. *, $P < 0.01$ vs control siRNA.

In the same vein, the increase of the band corresponding to LC3-II (Fig. 8B, bottom left panel), induced by HBSS in cells transfected with control siRNA was significantly reduced in cells transfected with *MFN2* siRNA. These results were also quantified by morphometric and densitometric analyses (Fig. 8B, right panels, bar graphs).

In addition, FRET analysis revealed that the CANX-AMBRA1 association induced by HBSS in fibroblasts transfected with control siRNA was significantly reduced in cells transfected with *MFN2* siRNA (Fig. 8C, middle panel). Statistical analysis, performed by the Riemann algorithm, revealed that the association CANX-AMBRA1 (expressed as FE) in *MFN2* siRNA-transfected cells was significantly lower than in control siRNA-transfected cells after autophagic triggering by HBSS (Fig. 8C, right panel). Since the CANX-AMBRA1 molecular association seems to represent a key event in the early phases of autophagosome formation, these data indicate that *MFN2* may be an important actor in the molecular scrambling between mitochondria and the ER,⁴⁷ at the MAM level.

Discussion

In the present work we suggest that the previously hypothesized contribution of MAMs in the formation of autophagy-associated vesicles aimed at the engulfment and recycling of altered organelles or misfolded proteins, i.e., autophagosomes,²⁸ could include the participation of lipid “rafts.” These seem not to merely represent further actors of the process but fundamental constituents of the MAMs, without which the correct assembly of the vesicles and the scrambling among organelles can be impaired and the autophagic process hindered. This is suggested by the experiments reported here and carried out with siRNA specific for the *ST8SIA1* mRNA leading to the ganglioside formation. This experimental condition leads to an impairment of the ER-mitochondria crosstalk and the subsequent autophagosome nucleation. It means that the suggested “interplay” between ER and mitochondria during the autophagic process induced by metabolic impairment is the result of a complex framework of events under control of several key molecular actors, such as the core-complex proteins but, also, some core-complex sphingolipids. Hence, the present results are in accord with the hypothesis that lipid rafts could represent a functional platform at the MAM level during the early steps of autophagic process.^{19,28} Cholesterol-rich microdomains, called lipid rafts, have already been suggested to play a role in several cellular processes of great relevance for cell survival or death. They exert: i) a catalytic function at the plasma membrane, e.g. allowing receptor-mediated death signals to take place.^{16,48,49} The recruitment of death receptors in these microdomains bolsters signaling pathways and is essential for apoptosis ignition.⁴⁹ In addition, ii) lipid raft components can move throughout the cell cytoplasm via cytoskeletal structural scaffold probably contributing to dynamic organelle structural remodeling;³⁴ iii) they can be detected at mitochondrial level (raft-like microdomains) contributing either to the cascade of events leading to apoptosis execution or to the changes of mitochondrial structural features leading to mitochondrial fission processes,^{17,50} but also, finally, iv) they are associated with autophagosome morphogenesis, either in the initiation or in the

maturation phases.²¹ In a few words, molecular interactions seem to take place easily inside the microdomains either at plasma membrane or at organelle membranes. Changes of organelle curvature leading to the formation of vesicles or the occurrence of morphogenetic modifications of organelles, such as mitochondrial fission, could be facilitated by the sphingolipid constituents.⁵⁰ Thus, with the present work we add a novel evidence on this matter by suggesting that the previously hypothesized presence of lipid rafts in the MAMs could be pivotal in the mitochondria-ER crosstalk leading to autophagosome formation.

This finding is not surprising because during ER stress, CANX palmitoylation is already reported.⁵¹ In fact, as a general rule, palmitoylation represents one of the critical molecular modifications for the embedding of proteins into raft scaffolds, including ER raft-like microdomains, where palmitoylated proteins are concentrated.⁵² Autophagy-related core interactors, whose recruitment to MAMs after autophagic stimulation has recently been reported by Hamasaki et al.,²⁸ have in fact been analyzed, i.e. taking into account the lipid rafts. The analysis of these lipid rafts-associated proteins can be referred as to the existence of a sort of “raftome,” i.e., an embedding structural “device” that acts inside the cell associating or recruiting interactor proteins of relevance in various subcellular processes, including autophagy. Under our experimental conditions, we found a molecular interaction of the ganglioside GD3, already considered as a paradigmatic “brick” of lipid rafts in certain cell types such as fibroblasts, with core-initiator proteins of autophagy, such as AMBRA1 and BECN1. It can be hypothesized that, under autophagic stimulation, a recruitment of these molecules into lipid rafts at the MAM level could take place. This could represent a prerequisite for membrane scrambling between mitochondria and ER, thus suggesting a function for MAMs in the earliest events leading to omegasome formation.²⁸

In fact, AMBRA1 constitutes a direct regulatory link between ULK1 (unc-51 like autophagy activating kinase 1) and BECN1-PIK3C3, which is required for core complex positioning and activity within the cell.^{31,45} In particular, AMBRA1 phosphorylation by the ULK1 kinase has been suggested as able to regulate the localization of the BECN1 complex to the omegasome.³¹ Under physiological conditions, a pool of AMBRA1 favors its interaction with mitochondrial BCL2 but, after autophagy induction, AMBRA1 is released from BCL2 (B-cell CLL/lymphoma 2) and recruited to BECN1, thus regulating BECN1-dependent autophagy.⁵³ Interestingly, AMBRA1 is also able to bind the autophagosome adapter LC3 through an LC3 interacting region (LIR) motif.⁵⁴ In our work we found that AMBRA1 is recruited to the BECN1 complex at the MAM level, where it can regulate autophagy by interacting with WIPI1 and with CANX, thus confirming its role in the early events of the autophagic process. In addition, we found that *MFN2*, the mitochondrial membrane protein that participates in mitochondrial fusion and contributes to the maintenance and operation of the mitochondrial network, represents an important actor in the molecular scrambling between mitochondria and ER,⁴⁷ and could also play a role in MAM formation participating to the autophagic process.

Levels of multiple lipid species, including several sphingolipids (ceramide, ganglioside GM3, GM2, GM1, GD3 and

GD1a), cardiolipin, cholesterol and cholesterol esters, are elevated in autophagic vacuole fractions and lysosomes.⁵⁵ Conversely, although sphingolipid metabolism has been linked to autophagy, its relevance appears still not well understood. Blocking autophagy by deletion of the *ATG7* (autophagy-related 7) gene, which is essential for autophagosome formation, leads to an increase of sphingolipid metabolites, whereas the overexpression of serine palmitoyltransferase to elevate de novo sphingolipid biosynthesis can induce autophagy.⁵⁶ Hence, it has been suggested that autophagic process could contribute to limit excessive sphingolipid levels so that dysfunctional autophagy may result in sphingolipid accumulation that may contribute to the pathogenesis of some diseases.⁵⁶⁻⁵⁸ For example, In Alzheimer disease, abnormal sphingolipid metabolism leads to defective autophagic degradation due to impaired lysosomal biogenesis.⁵⁹ Hence, although surely representing key actors of autophagosomal biogenesis, the comprehension of the role of sphingolipid trafficking and their contribution to the autophagic flux is still at the beginning. In few words, the core ATG proteins can be functionally categorized into several units: the ATG1-ULK1 complex, the PtdIns3K complex, the ATG2-ATG18-WIPI complex, the ATG12 conjugation system and the LC3 conjugation system, but where the lipid molecules for autophagosomal membrane biogenesis come from is still unknown. In view of the molecular association we found between AMBRA1 and ganglioside GD3 in MAMs we can hypothesize that, under autophagic stimulation, the ER could provide a sphingolipid scaffold, MAM “rafts,” where early autophagy-related molecules are recruited, i.e. favoring the interaction of key proteins of the core-complex. In conclusion, we suggest that the observed molecular interaction GD3-AMBRA1, under autophagic stimulation, and conversely the lack of interaction at the MAM level between key initiators of autophagy in the presence of *ST8SIA1* siRNA, i.e., CANX-AMBRA1, could indicate that MAM raft-like microdomains could be pivotal in the initial organelle scrambling activity that finally leads to the formation of an autophagosome.

Materials and methods

Cells and autophagy induction

Primary human skin cultured fibroblasts were available at the bio-bank of our laboratories and were established from biopsies of sun-protected forearm skin according to standard culture methods. All the donors gave their informed consent before biopsy was performed. All the analyses were performed on cells between 3rd and 7th passage of culture at nearly 90% confluence.^{21,60} No significant variability among samples from different individuals was observed. The model represented by primarily cultured cells represents, in comparison with cell lines, a more valuable experimental tool. In particular, we previously showed that cultured fibroblasts represent a suitable cell model for studying the role of lipid rafts in autophagosome formation.²¹ Cell cultures were maintained in Dulbecco's modified Eagle's medium (DMEM; Sigma, D5796), containing 10% fetal calf serum (FCS) plus 100 units/ml penicillin, 10 mg/ml streptomycin, at 37°C in a humidified CO₂ atmosphere. For autophagy induction, cells were stimulated under condition of nutrient

deprivation with HBSS (Sigma, H9269) for 1 h at 37°C. The optimal incubation time with HBSS was selected on the basis of preliminary experiments. After treatment, cells were collected and prepared for the experimental procedures described below.

Analysis of autophagy

Flow cytometry analyses. Evaluation of autophagy was performed by using a Cyto-ID Autophagy Detection Kit (Enzo Life Sciences, ENZ-51031-K200). The kit was optimized for detection of autophagy in live cells by flow cytometry. This assay provides a rapid, specific and quantitative approach for monitoring autophagic activity at the cellular level by using a 488 nm-excitable probe that becomes fluorescent in vesicles produced during autophagy.⁶¹

Immunofluorescence. Cells (untreated or treated with HBSS), fixed with 4% paraformaldehyde and permeabilized by 0.5% (v/v) Triton X-100 (Bio-Rad, 161-0407) were incubated with rabbit PAb anti-LC3 antibody (Abgent, AP1805A) for 1 h at 4°C, followed by Alexa Fluor 488-conjugated anti-rabbit (Molecular Probes, A-11008) for an additional 30 min. Finally, after washing, all samples were counterstained with Hoechst 33258 (Sigma, 94403), 1 mg/ml in phosphate-buffered saline (PBS; Sigma, P4417), and then mounted in glycerol:PBS (ratio 1:1, pH 7.4). The images were acquired by intensified video microscopy (IVM) with an Olympus fluorescence microscope (*Olympus Corporation of the Americas, Center Valley, Pa.*), equipped with a Zeiss charge-coupled device camera (Carl Zeiss, Oberkochen, Germany). For morphometric analyses by fluorescence microscopy, LC3 puncta positive cells were calculated as a percentage by counting directly under the microscope (objective 60x) at least 200 cells per sample.

Western blot analysis. Cells, untreated or treated with HBSS for 1 h at 37°C, were lysed in lysis buffer containing 1% Triton X-100, 10 mM Tris-HCl, pH 7.5, 150 mM NaCl, 5 mM EDTA, 1 mM Na₃VO₄ and 75 U of aprotinin (Sigma, A1153) and allowed to stand for 20 min at 4°C. The cell suspension was mechanically disrupted by Dounce (Wheaton Industries Inc., NJ, USA, 357538) homogenization (10 strokes). The lysate was centrifuged for 5 min at 1300xg to remove nuclei and large cellular debris. After evaluation of the protein concentration by Bradford Dye Reagent assay (Bio-Rad, 500-0006), the lysate was subjected to 15% sodium-dodecyl sulfate polyacrylamide gel electrophoresis (SDS-PAGE). The proteins were electrophoretically transferred onto polyvinylidene difluoride (PVDF) membranes (Bio-Rad, 162-0177). Membranes were blocked with 5% nonfat dried milk in TBS (Bio-Rad, 1706435), containing 0.05% Tween 20 (Bio-Rad, 1706531) and probed with rabbit PAb anti-LC3 antibody (MBL Int Corporation, PD014), with rabbit anti-phospho-ULK1 (Ser757) PAb (Cell Signaling Technology, 6888) or with anti-ACTB (actin, β) MAb (Sigma, A5316). Bound antibodies were visualized with horseradish peroxidase (HRP)-conjugated anti-rabbit IgG (Sigma, A1949) or anti-mouse IgG (Sigma, A9044) and immunoreactivity assessed by chemiluminescence reaction, using the ECL western detection system (Amersham, RPN2106). Densitometric scanning analysis was performed with Mac OS X (Apple Computer International), using NIH ImageJ 1.62 software. The

density of each band in the same gel was analyzed and the densitometric LC3-II/ACTB ratios are shown.

Sucrose-gradient fractionation and immunoblotting analysis

Lipid raft fractions were isolated as previously described.¹⁷ Briefly, cell lysates were centrifuged for 5 min at 1300xg. The supernatant fraction (postnuclear fraction) was subjected to linear sucrose density gradient (5–30%) centrifugation. After centrifugation, the gradient was fractionated, and 11 fractions were collected starting from the top of the tube. The fraction samples were loaded by volume and subjected to SDS-PAGE. The proteins were electrophoretically transferred onto PVDF membranes and probed with anti-CANX mAb (Abcam, ab31290) or with anti-VDAC1 (Santa Cruz Biotechnology, sc-8828) PAb antibodies. Bound antibodies were visualized with HRP-conjugated anti-mouse IgG (Amersham, NA931V) or anti-goat IgG (Dako, P0449) and immunoreactivity was assessed by chemiluminescence reaction, using the ECL western detection system.

Transmission electron microscopy and immunoelectron microscopy (IEM)

For TEM examination, control and autophagy-stimulated cells were fixed in 2.5% cacodylate-buffered (0.2 M, pH 7.2) glutaraldehyde for 20 min at room temperature and postfixed in 1% OsO₄ in cacodylate buffer for 1 h at room temperature. Fixed specimens were dehydrated through a graded series of ethanol solutions and embedded in Agar 100 (Agar Aids, AG-R1031). Ultrathin sections were collected on 200-mesh gold grids and treated with PBS containing 1% (w/v) gelatin (TAAB, B042), 1% BSA (TAAB, B041), 5% FCS and 0.05% Tween 20 and then incubated with IgG anti-GD3 R24 MAb (Abcam, ab11779), diluted 1:10 in the same buffer without gelatin overnight at 4°C. After washing for 1 h at room temperature, sections were labeled with protein A-10 nm gold conjugate (1:10;TAAB, GEM020/1) for 1 h at room temperature and washed again. Negative controls were incubated with the gold conjugate alone. Sections were observed with a Philips 208 electron microscope (FEI Company, Achtseweg Noord 5, Bldg 5651 GG Eindhoven, The Netherlands) at 80 kV. Morphometric analyses were performed by evaluating the percentage of cells in which ER was adjacent to mitochondria as well as of cells in which there are small rounded vesicles in the proximity of mitochondria either in fed or in HBSS-treated cells. At least 100 cells per sample were analyzed at the same magnification (10000x).

Ganglioside immunostaining

Briefly, aliquots, obtained from MAM fractions or from CANX, AMBRA1 or SEL1L, immunoprecipitates, prepared as above, were spotted onto nitrocellulose strips, which were allowed to dry at room temperature. The strips were blocked with 5% nonfat dried milk in TBS, containing 0.05% Tween 20 for 1 h to block the residual binding sites on the paper. The strips were rinsed for 10 min in TBS-Tween and then incubated with IgG anti-GD3 R24 mAb (Abcam, ab 11779)

for 1 h at room temperature. After incubation the strips were washed in PBS and further incubated for 1 h at 37°C with HRP-conjugated anti-mouse IgG. Immunoreactivity was assessed by chemiluminescence reaction, using the ECL western detection system.

Immunoprecipitation experiments

Cells, untreated or treated with HBSS for 1 h at 37°C, were lysed in lysis buffer (10 mM Tris-HCl, pH 8.0, 150 mM NaCl, 1% Nonidet P-40 [Sigma, 213277], 1 mM phenylmethylsulfonyl fluoride [Sigma, P7626], 10 mg/ml leupeptin [Sigma, L2884]). Cell-free lysates were mixed with protein G-acrylic beads (Sigma, P3296) and stirred by a rotary shaker for 2 h at 4°C to preclude nonspecific binding. After centrifugation (500xg for 1 min), the supernatant fraction was immunoprecipitated with rabbit anti-CANX PAb (Sigma, C4731), rabbit anti-AMBRA1 PAb (Covalab, 0224), or rabbit anti-SEL1 PAb (Abcam, ab78298) plus protein G-acrylic beads. After vigorous mixing for 5 min, samples were further mixed. As a negative control, immunoprecipitation was performed with an irrelevant rabbit IgG (Sigma, 15006). The immunoprecipitates were split into 2 aliquots. The first one was subjected to dot blot analysis for GD3 detection; the second one was checked by western blot analysis.

Immunoblotting analysis of immunoprecipitates

The immunoprecipitates, obtained as reported above, were subjected to SDS-PAGE. The proteins were electrophoretically transferred onto PVDF membranes. Membrane were blocked with 5% nonfat dried milk in TBS, containing 0.05% Tween 20 and probed with: mouse anti-AMBRA1 MAb (Santa Cruz Biotechnology, sc-398204), rabbit anti-WIPI1 PAb (Bioss, ABIN750418), rabbit anti-ATG16L1 PAb (MBL, PM040), rabbit anti-WIPI2 PAb (GeneTex, GTX122101), mouse anti-CANX mAb (Abcam, ab31290), rabbit anti-POR PAb (Abcam, ab39995), anti-SEL1 MAb (MyBioSource MBS604203), rabbit anti-PIK3C3 PAb (Cell Signaling Technology, 3811), rabbit anti-BECN1 PAb (Santa Cruz Biotechnology, sc-11427), rabbit anti-ATG14 PAb (Abcam, ab-173943), or rabbit anti-UVRAG PAb (Abgent, ap-1850d). Bound antibodies were visualized with HRP-conjugated anti-mouse IgG or anti-rabbit IgG (Sigma, A1949) and immunoreactivity assessed by chemiluminescence reaction, using the ECL western detection system.

Quantitative fluorescence resonance energy transfer (FRET) analysis

We applied fluorescence resonance energy transfer (FRET) analysis by flow cytometry, in order to study the molecular association of: GD3-AMBRA1, GD3-CANX, GD3-WIPI1, GD3-SEL1, AMBRA1-WIPI1, AMBRA1-WIPI2, CANX-AMBRA1, CANX-WIPI1, CANX-WIPI2, CANX-ATG16L1.

The following primary and secondary antibodies used were: rabbit PAb anti-CANX (Sigma, C4731), mouse anti-CANX mAb (Abcam, ab31290), rabbit PAb anti-AMBRA1 (Covalab, 0224), rabbit PAb anti-SEL1 (Abcam, ab78298), rabbit anti-P4HB PAb (Abcam, ab31811), rabbit anti-WIPI1 PAb (Bioss,

ABIN750418), rabbit anti-ATG16L1 PAb (MBL, PM040), rabbit anti-WIPI2 PAb (GeneTex, GTX122101), mouse MAb anti-WIPI2 (Abcam, ab105459), anti-mouse PE-conjugated (BD PharMingen, 550589), anti-mouse Cy5-conjugated (Abcam, ab6563); anti-rabbit PE-conjugated (BD PharMingen, 558416), anti-rabbit Cy5 conjugated (Abcam, ab97077).

Briefly, cells were fixed and permeabilized as above, washed twice in cold PBS and then labeled with antibodies tagged with donor (phycoerythrin, PE) or acceptor (Cy5) dyes. Cell staining was performed using mouse or rabbit primary antibodies and saturating amount of PE-labeled anti-mouse or anti-rabbit. In a second step, primary antibodies were detected by using specific secondary antibodies followed by saturating concentrations of Cy5-conjugated anti-mouse or anti-rabbit. After staining, cells were washed twice, resuspended in PBS and analyzed with a dual-laser FACScalibur flow cytometer (BD Biosciences Franklin Lakes, New Jersey). For determination of FRET efficiency (FE), changes in fluorescence intensities of donor plus acceptor labeled cells were compared to the emission signal from cells labeled with donor-only and acceptor-only fluorophores. As a further control, the cross-reactivity among all the different primary and secondary antibodies was also assessed. All data were corrected for background by subtracting the binding of the isotype controls. Efficient energy transfer resulted in an increased acceptor emission on cells stained with both donor and acceptor dyes. The FE was calculated according to Riemann.⁶²

Isolation of MAMs

Crude mitochondria, obtained from cells as previously reported,⁶³ either untreated or treated with HBSS for 1 h at 37°C, were fractionated to isolate high-purity MAM and mitochondria fractions according to Wieckowski et al.⁶⁴ Briefly, crude mitochondrial pellets were resuspended in 2 ml of ice cold mitochondria resuspending buffer (MRB), containing 250 mM mannitol, 5 mM HEPES, pH 7.4, and 0.5 mM EGTA and loaded on top of 8 ml of Percoll medium (225 mM mannitol, 25 mM HEPES, pH 7.4, 1 mM EGTA, and 30% Percoll [vol/vol; Sigma, P1644]) in an ultracentrifuge tube. Afterward, the tube was gently filled up with 3.5 ml of MRB solution and centrifuged at 95,000 × g for 30 min at 4°C in an SW 41 rotor (Beckman Coulter, Brea, CA, USA). After centrifugation, a dense band containing purified mitochondria was localized approximately at the bottom, whereas the MAM fraction was visible as diffuse white band located above the mitochondria. The fractions were collected and centrifuged at 6300 × g for 10 min at 4°C. The MAM supernatant was subjected to a further centrifugation at 100,000 × g for 1 h at 4°C in a 70-Ti rotor (Beckman Coulter, Brea, CA, USA). After evaluation of the protein concentration by the Bradford Dye Reagent assay, MAM fractions were analyzed by western blot analysis using anti-AMBRA1 mAb, anti-WIPI1 PAb, anti-ATG16L1 PAb and anti-WIPI2 PAb. Bound antibodies were visualized with HRP-conjugated anti-mouse IgG or anti-rabbit IgG and immunoreactivity assessed by chemiluminescence reaction, using the ECL western detection system. Subcellular fractions, including MAM as well as pure mitochondria, isolated from cells, either untreated or treated with HBSS, were tested for the

mitochondrial marker, using anti-TOMM20 MAb (Abcam, ab56783), for the ER marker using anti-P4HB PAb (Abcam, ab31811), for the MAM markers using anti-CANX mAb and anti-VDAC1 PAb antibodies.

Knockdown experiments with siRNA

Primary fibroblasts were cultured in an antibiotic-free medium containing 10% FCS and transfected with Dharma FECT 1 reagent (Dharmacon, T-2001-03), according to the manufacturer's instructions, using 25 nM of Smart pool siRNA *ST8SIA1* (GD3 synthase) (Dharmacon, M-011775-02). As further control we used Smart pool siRNA *ATG5* (positive control, Dharmacon, M-004374-04) or related scrambled siRNA as negative control (Dharmacon, D-001810-10-05). The transfection efficiency was confirmed by using a Dharmacon's positive silencing control, siGLO *LMNA* (lamin A/C) siRNA (D-001620-02). For knocking down MFN2, we transfected fibroblasts with a predesigned siRNA directed against human MFN2 (FlexiTube GeneSolution, Qiagen, GS9927) by using HiPerFect Transfection Reagent (Qiagen, 301705) according to the manufacturer's instructions. As a negative control, we used a nonsilencing siRNA with no homology to any known mammalian gene (All-Stars Negative Control siRNA, Qiagen, SI03650318). The transfection efficiency was verified by a GFP-22 siRNA (Qiagen, 1022064). After 48 h, the effect of transfection on *ST8SIA1*, *ATG5*, or *MFN2* expression levels was verified by flow cytometry by using a rabbit anti-*ST8SIA1* (K-18) PAb (Santa Cruz Biotechnology, sc-44587), by a rabbit anti-*ATG5* (Sigma-Aldrich, HPA042973) PAb, or by a rabbit anti-*MFN2* (D1E9) MAb (Cell Signaling Technology, 11925).

Forty-eight h after transfection cells were treated with HBSS for 1 h as described above and then analyzed by flow cytometry, fluorescence microscopy and western blot.

Data analysis and statistics

For flow cytometry studies all samples were analyzed by a dual-laser FACScalibur cytometer equipped with a 488 argon laser and with a 635 red diode laser. At least 20,000 events/sample were acquired. Data were recorded and statistically analyzed with a Macintosh computer using CellQuestPro Software. Collected data analysis was carried out by using ANOVA 2-way test for repeated samples by using Graphpad Prism software corrected for multiple comparisons by the Bonferroni procedure. All data reported in this paper were verified in at least 3 different experiments and reported as mean ± standard deviation (SD). Only *P* values of less than 0.01 were considered as significant.

Abbreviations

ACTB	actin, β
AMBRA1	autophagy/Beclin 1 regulator 1
ATG5	autophagy-related 5
ATG14	autophagy-related 14, ATG16L1, autophagy-related 16 like 1
BECN1	Beclin 1, autophagy related
CANX	calnexin

Cy5	cyanine5
ECL	enhanced chemiluminescence
ER	endoplasmic reticulum
FE	FRET efficiency
FRET	fluorescence resonance energy transfer
GD3	aNeu5Ac(2-8)aNeu5Ac(2-3)bDGalp(1-4)bDGlcp(1-1)ceramide
GM1	monosialotetrahexosylganglioside
GSLs	glycosphingolipids
HBSS	Hank's balanced salt solution
HRP	horseradish peroxidase
IEM	immunoelectron microscopy
IVM	intensified video microscopy
LMNA	lamin A/C
MAb	monoclonal antibody
MAMs	mitochondria-associated membranes
MAP1LC3/LC3B	microtubule associated protein 1 light chain 3
MFN2	mitofusin 2
P-ULK1	phosphorylated ULK1
P4HB	prolyl 4-hydroxylase subunit β
PAb	polyclonal antibody
PE	phycoerythrin
PIK3C3	phosphatidylinositol 3-kinase catalytic subunit type 3
POR	P450 (cytochrome) oxidoreductase
PtdIns3K	class III phosphatidylinositol 3-kinase
PtdIns3P	phosphatidylinositol 3-phosphate
SD	standard deviation
SEL1L	SEL1L ERAD E3 ligase adaptor subunit
ST8SIA1/GD3 synthase	ST8 α -N-acetyl-neuraminide α -2,8-sialyltransferase 1
TEM	transmission electron microscopy
TOMM20	translocase of outer mitochondrial membrane 20 homolog (yeast)
ULK1	unc-51 like autophagy activating kinase 1
UVRAG	UV radiation resistance associated
VDAC1	voltage dependent anion channel 1
WIPI1	WD repeat domain, phosphoinositide interacting 1
WIPI2	WD repeat domain, phosphoinositide interacting 2

Disclosure of potential conflicts of interest

No potential conflicts of interest were disclosed.

Funding

This work was supported in part by grants from the Ministry of Education, University and Research (Rome, Italy), the Ministry of Health (WM; PM), the Italian Association for Cancer Research (MCO-9998 and 11505) (WM); Arcobaleno Onlus (WM); Peretti Foundation (WM); PRIN project 2009 (MS); PRIN project 2011 (RM) and Sapienza University project 2013-2014 (MS).

References

- Goetz JG, Nabi IR. Interaction of the smooth endoplasmic reticulum and mitochondria. *Biochem Soc Trans* 2006; 34:370-3; PMID:16709164; <http://dx.doi.org/10.1042/BST0340370>
- Raturi A, Simmen T. Where the endoplasmic reticulum and the mitochondrion tie the knot: The mitochondria-associated membrane (MAM) *Biochim Biophys Acta* 2013; 1833:213-24; PMID:22575682; <http://dx.doi.org/10.1016/j.bbamcr.2012.04.013>
- Kornmann B. The molecular hug between the ER and the mitochondria. *Curr Opin Cell Biol* 2013; 25:443-8; <http://dx.doi.org/10.1016/j.ceb.2013.02.010>
- Franke WW, Kartenbeck J. Outer mitochondrial membrane continuous with endoplasmic reticulum. *Protoplasma* 1971; 73:35-41; PMID:5000179; <http://dx.doi.org/10.1007/BF01286409>
- Morré DJ, Merritt WD, Lembi CA. Connections between mitochondria and endoplasmic reticulum in rat liver and onion stem. *Protoplasma* 1971; 73:43-9; <http://dx.doi.org/10.1007/BF01286410>
- Copeland DE, Dalton AJ. An association between mitochondria and the endoplasmic reticulum in cells of the pseudobranch gland of a teleost. *J Biophys Biochem Cytol* 1959; 5:393-6; PMID:13664679; <http://dx.doi.org/10.1083/jcb.5.3.393>
- Lewis LA, Tata JR. A rapidly sedimenting fraction of rat liver endoplasmic reticulum. *J Clin Sci* 1973; 13: 447-59.
- Meier PJ, Spycher MA, Meyer UA. Isolation and characterization of rough endoplasmic reticulum associated with mitochondria from normal rat liver. *Biochim Biophys Acta* 1981; 646:283-97; PMID:6170330; [http://dx.doi.org/10.1016/0005-2736\(81\)90335-7](http://dx.doi.org/10.1016/0005-2736(81)90335-7)
- Pickett CB, Montisano D, Cascarno J. The physical association between rat liver mitochondria and rough endoplasmic reticulum. Isolation, electron microscopic examination and sedimentation equilibrium centrifugation analyses of rough endoplasmic reticulum-mitochondrial complexes. *Exp Cell Res* 1980; 128:343-52; PMID:7408995; [http://dx.doi.org/10.1016/0014-4827\(80\)90070-1](http://dx.doi.org/10.1016/0014-4827(80)90070-1)
- Katz J, Wals PA, Golden S, Rajman L. Mitochondrial-reticular cytostructure in liver cells. *Biochem J* 1983; 214:795-813; PMID:6354178; <http://dx.doi.org/10.1042/bj2140795>
- Vance JE. MAM (mitochondria-associated membranes) in mammalian cells: lipids and beyond. *Biochim Biophys Acta* 2014; 1841:595-609; PMID:24316057; <http://dx.doi.org/10.1016/j.bbali.2013.11.014>
- Vance JE. Phospholipid synthesis in a membrane fraction associated with mitochondria. *J Biol Chem* 1990; 265:7248-56.
- Levine T. Short-range intracellular trafficking of small molecules across endoplasmic reticulum junctions. *Trends Cell Biol* 2004; 14:483-90; PMID:15350976; <http://dx.doi.org/10.1016/j.tcb.2004.07.017>
- Hayashi T, Fujimoto M. Detergent-resistant microdomains determine the localization of sigma-1 receptors to the endoplasmic reticulum-mitochondria junction. *Mol Pharmacol* 2010; 77:517-28; PMID:20053954; <http://dx.doi.org/10.1124/mol.109.062539>
- Annunziata I, d'Azzo A. Interorganellar Membrane Microdomains: Dynamic Platforms in the Control of Calcium Signaling and Apoptosis. *Cells* 2013; 2:574-90; PMID:24709798; <http://dx.doi.org/10.3390/cells2030574>
- Simons K, Ikonen, E. Functional rafts in cell membranes. *Nature* 1997; 387:569-72. PMID:9177342; <http://dx.doi.org/10.1038/42408>
- Garofalo T, Giammarioli AM, Misasi R, Tinari A, Manganelli V, Gambardella L, Pavan A, Malorni W, Sorice M. Lipid microdomains contribute to apoptosis-associated modifications of mitochondria in T cells. *Cell Death Differ* 2005; 12:1378-89; PMID:15947792; <http://dx.doi.org/10.1038/sj.cdd.4401672>
- Browman DT, Resek ME, Zajchowski LD, Robbins SM. Erlin-1 and erlin-2 are novel members of the prohibitin family of proteins that define lipid-raft-like domains of the ER. *J Cell Sci* 2006; 119:3149-60; PMID:16835267; <http://dx.doi.org/10.1242/jcs.03060>
- Sano R, Annunziata I, Patterson A, Moshiah S, Gomero E, Opferman J, Forte M, d'Azzo A. GM1-ganglioside accumulation at the mitochondria-associated ER membranes links ER stress to Ca(2+)-dependent mitochondrial apoptosis. *Mol Cell* 2009; 36:500-11; PMID:19917257; <http://dx.doi.org/10.1016/j.molcel.2009.10.021>

- [20] Garofalo T, Manganelli V, Grasso M, Mattei V, Ferri A, Misasi R, Sorice M. Role of mitochondrial raft-like microdomains in the regulation of cell apoptosis. *Apoptosis* 2015; 20(5):621-34; PMID:25652700
- [21] Matarrese P, Garofalo T, Manganelli V, Gambardella L, Marconi M, Grasso M, Tinari A, Misasi R, Malorni W, Sorice M. Evidence for the involvement of GD3 ganglioside in autophagosome formation and maturation. *Autophagy* 2014; 10:750-65; PMID:24589479; <http://dx.doi.org/10.4161/auto.27959>
- [22] Mizushima N, Yoshimori T, Ohsumi Y. The role of Atg proteins in autophagosome formation. *Annu Rev Cell Dev Biol* 2011; 27:107-32; PMID:21801009; <http://dx.doi.org/10.1146/annurev-cellbio-092910-154005>
- [23] Tooze SA, Yoshimori T. The origin of the autophagosomal membrane. *Nature Cell Biol* 2010; 12:831-5; PMID:20811355; <http://dx.doi.org/10.1038/ncb0910-831>
- [24] Matsunaga K, Morita E, Saitoh T, Akira S, Ktistakis NT, Izumi T, Noda T, Yoshimori T. Autophagy requires endoplasmic reticulum targeting of the PI3-kinase complex via Atg14L. *J Cell Biol* 2010; 190:511-21; PMID:20713597; <http://dx.doi.org/10.1083/jcb.200911141>
- [25] Hayashi-Nishino M, Fujita N, Noda T, Yamaguchi A, Yoshimori T, Yamamoto A. A subdomain of the endoplasmic reticulum forms a cradle for autophagosome formation. *Nature Cell Biol* 2009; 11:1433-7; PMID:19898463; <http://dx.doi.org/10.1038/ncb1991>
- [26] Yla-Anttila P, Vihinen H, Jokitalo E, Eskelinen EL. 3D tomography reveals connections between the phagophore and endoplasmic reticulum. *Autophagy* 2009; 5:1180-5; PMID:19855179; <http://dx.doi.org/10.4161/auto.5.8.10274>
- [27] Hailey DW, Rambold AS, Satpute-Krishnan P, Mitra K, Sougrat R, Kim PK, Lippincott-Schwartz J. Mitochondria supply membranes for autophagosome biogenesis during starvation. *Cell* 2010; 141:656-67; PMID:20478256; <http://dx.doi.org/10.1016/j.cell.2010.04.009>
- [28] Hamasaki M, Furuta N, Matsuda A, Nezu A, Yamamoto A, Fujita N, Oomori H, Noda T, Haraguchi T, Hiraoka Y, Amano A, Yoshimori T. Autophagosomes form at ER-mitochondria contact sites. *Nature* 2013; 495:389-93; PMID:23455425; <http://dx.doi.org/10.1038/nature11910>
- [29] Kihara A, Kabeja Y, Ohsumi Y, Yoshimori T. Beclin-phosphatidylinositol 3-kinase complex functions at the *trans*-Golgi network. *EMBO Rep* 2001; 2:330-5; PMID:11306555; <http://dx.doi.org/10.1093/embo-reports/kve061>
- [30] Fimia GM, Stoykova A, Romagnoli A, Giunta L, Di Bartolomeo S, Nardacci R, Corazzari M, Fuoco C, Ucar A, Schwartz P, Gruss P, Piacentini M, Chowdhury K, Cecconi F. Ambra1 regulates autophagy and development of the nervous system. *Nature* 2007; 447:1121-5; PMID:17589504
- [31] Fimia GM, Di Bartolomeo S, Piacentini M, Cecconi F. Unleashing the Ambra1-Beclin1 complex from dynein chains: Ulk1 sets Ambra1 free to induce autophagy. *Autophagy* 2011; 7:115-7; PMID:21079415; <http://dx.doi.org/10.4161/auto.7.1.14071>
- [32] Giammarioli AM, Garofalo T, Sorice M, Misasi R, Gambardella L, Gradini R, Fais S, Pavan A, Malorni W. GD3 glycosphingolipid contributes to Fas-mediated apoptosis via association with ezrin cytoskeletal protein. *FEBS Lett* 2001; 506:45-50; PMID:11591368; [http://dx.doi.org/10.1016/S0014-5793\(01\)02776-4](http://dx.doi.org/10.1016/S0014-5793(01)02776-4)
- [33] Sorice M, Matarrese P, Tinari A, Giammarioli AM, Garofalo T, Manganelli V, Ciarlo L, Gambardella L, Maccari G, Botta M, Misasi R, Malorni W. Raft component GD3 associates with tubulin following CD95/Fas ligation. *FASEB J* 2009; 23:3298-308; PMID:19509307; <http://dx.doi.org/10.1096/fj.08-128140>
- [34] Sorice M, Matarrese P, Manganelli V, Tinari A, Giammarioli AM, Mattei V, Misasi R, Garofalo T, Malorni W. Role of GD3-CLIPR-59 association in lymphoblastoid T cell apoptosis triggered by CD95/Fas. *Plos One* 2010; 5:e8567; PMID:20052288; <http://dx.doi.org/10.1371/journal.pone.0008567>
- [35] Sorice M, Mattei V, Tasciotti V, Manganelli V, Garofalo T, Misasi R. Trafficking of PrPc to mitochondrial raft-like microdomains during cell apoptosis. *Prion* 2012; 6:354-8; PMID:22842913; <http://dx.doi.org/10.4161/pri.20479>
- [36] Mattei V, Matarrese P, Garofalo T, Tinari A, Gambardella L, Ciarlo L, Manganelli V, Tasciotti V, Misasi R, Malorni W, Sorice M. Recruitment of cellular prion protein to mitochondrial raft-like microdomains contributes to apoptosis execution. *Mol Biol Cell* 2011; 22: 4842-53; PMID:22031292; <http://dx.doi.org/10.1091/mbc.E11-04-0348>
- [37] Garcia-Ruiz C, Colell A, Morales A, Calva M, Enrich C, Fernandez-Checa JC. Trafficking of ganglioside GD3 to mitochondria by tumor necrosis factor- α . *J Biol Chem* 2002; 277:36443-8; PMID:12118012; <http://dx.doi.org/10.1074/jbc.M206021200>
- [38] Myhill N, Lynes EM, Nanji JA, Blagoveshchenskaya AD, Fei H, Carmine Simmen K, Cooper TJ, Thomas G, Simmen T. The subcellular distribution of calnexin is mediated by PACS-2. *Mol Biol Cell* 2008; 19:2777-88; PMID:18417615; <http://dx.doi.org/10.1091/mbc.E07-10-0995>
- [39] Proikas-Cezanne T, Ruckerbauer S, Stierhof YD, Berg C, Nordheim A. Human WIPI-1 puncta-formation: a novel assay to assess mammalian autophagy. *FEBS Lett* 2007; 581:3396-404; PMID:17618624; <http://dx.doi.org/10.1016/j.febslet.2007.06.040>
- [40] Lamb CA, Yoshimori T, Tooze SA. The autophagosome: origins unknown, biogenesis complex. *Nat Rev Mol Cell Biol* 2013; 14:759-74; PMID:24201109; <http://dx.doi.org/10.1038/nrm3696>
- [41] Malorni W, Giammarioli AM, Garofalo T, Sorice M. Dynamics of lipid raft components during lymphocyte apoptosis: the paradigmatic role of GD3. *Apoptosis* 2007; 12:941-49; PMID:17453161; <http://dx.doi.org/10.1007/s10495-007-0757-1>
- [42] Lilley BN, Ploegh HL. Multiprotein complexes that link dislocation, ubiquitination, and extraction of misfolded proteins from the endoplasmic reticulum membrane. *Proc Natl Acad Sci U S A* 2005; 102:14296-301; PMID:16186509; <http://dx.doi.org/10.1073/pnas.0505014102>
- [43] Dooley HC, Razi M, Polson HE, Girardin SE, Wilson MI, Tooze SA. WIPI2 links LC3 conjugation with PI3P, autophagosome formation, and pathogen clearance by recruiting Atg12-5-16L1. *Mol Cell* 2014; 55:238-52; PMID:24954904; <http://dx.doi.org/10.1016/j.molcel.2014.05.021>
- [44] Hortsch M, Meyer DI. Immunochemical analysis of rough and smooth microsomes from rat liver. Segregation of docking protein in rough membranes. *Eur J Biochem* 1985; 150:559-64; PMID:4018097; <http://dx.doi.org/10.1111/j.1432-1033.1985.tb09057.x>
- [45] Funderburk SF, Wang QJ, Yue Z. The Beclin 1-VPS34 complex—at the crossroads of autophagy and beyond. *Trends Cell Biol* 2010; 20:355-62; PMID:20356743; <http://dx.doi.org/10.1016/j.tcb.2010.03.002>
- [46] Sugiura A, Nagashima S, Tokuyama T, Amo T, Matsuki Y, Ishido S, Kudo Y, McBride HM, Fukuda T, Matsushita N, Inatome R, Yanagi S. MITOL regulates endoplasmic reticulum-mitochondria contacts via Mitofusin2. *Mol Cell* 2013; 51:20-34; PMID:23727017; <http://dx.doi.org/10.1016/j.molcel.2013.04.023>
- [47] de Brito OM, Scorrano L. Mitofusin-2 regulates mitochondrial and endoplasmic reticulum morphology and tethering: the role of Ras. *Mitochondrion* 2009; 9:222-26; PMID:19269351; <http://dx.doi.org/10.1016/j.mito.2009.02.005>
- [48] Scheel-Toellner D, Wang K, Singh R, Majeed S, Raza K, Curnow SJ, Salmon M, Lord JM. The death-inducing signaling complex is recruited to lipid rafts in Fas-induced apoptosis. *Biochem Biophys Res Commun* 2002; 297:876-79; PMID:12359234; [http://dx.doi.org/10.1016/S0006-291X\(02\)02311-2](http://dx.doi.org/10.1016/S0006-291X(02)02311-2)
- [49] Garofalo T, Misasi R, Mattei V, Giammarioli AM, Malorni W, Pontieri GM, Pavan A, Sorice M. Association of the death-inducing signaling complex with microdomains after triggering through CD95/Fas. Evidence for caspase-8-ganglioside interaction in T cells. *J Biol Chem* 2003; 278:8309-315; PMID:12499380; <http://dx.doi.org/10.1074/jbc.M207618200>
- [50] Ciarlo L, Manganelli V, Garofalo T, Matarrese P, Tinari A, Misasi R, Malorni W, Sorice M. Association of fission proteins with mitochondrial raft-like domains. *Cell Death Differ* 2010; 17:1047-58; PMID:20075943; <http://dx.doi.org/10.1038/cdd.2009.208>

- [51] Strappazzon F, Vietri-Rudan M, Campello S, Nazio F, Florenzano F, Fimia GM, Piacentini M, Levine B, Cecconi F. Mitochondrial BCL-2 inhibits AMBRA1-induced autophagy. *EMBO J* 2011; 30:1195-208; PMID:21358617; <http://dx.doi.org/10.1038/emboj.2011.49>
- [52] Strappazzon F, Nazio F, Corrado M, Cianfanelli V, Romagnoli A, Fimia GM, Campello S, Nardacci R, Piacentini M, Campanella M, Cecconi F. Mitochondrial BCL-2 inhibits AMBRA1-induced autophagy. *Cell Death Differ* 2015; 22:419-32; PMID:25215947; <http://dx.doi.org/10.1038/cdd.2014.139>
- [53] Lynes EM, Raturi A, Shenkman M, Ortiz Sandoval C, Yap MC, Wu J, Janowicz A, Myhill N, Benson MD, Campbell RE, et al. Palmitoylation is the switch that assigns calnexin to quality control or ER Ca²⁺ signaling. *J Cell Sci* 2013; 126:3893-903; PMID:23843619; <http://dx.doi.org/10.1242/jcs.125856>
- [54] Linder ME, Deschenes RJ. Palmitoylation: Policing protein stability and traffic. *Nat Rev Mol Cell Biol* 2007; 8:74-84; <http://dx.doi.org/10.1038/nrm2084>
- [55] Yang DS, Stavrides P, Saito M, Kumar A, Rodriguez-Navarro JA, Pawlik M, Huo C, Walkley SU, Saito M, Cuervo AM, et al. Defective macroautophagic turnover of brain lipids in the TgCRND8 Alzheimer mouse model: prevention by correcting lysosomal proteolytic deficits. *Brain* 2014; 137: 3300-318; PMID:25270989; <http://dx.doi.org/10.1093/brain/awu278>
- [56] Alexaki A, Gupta SD, Majumder S, Kono M, Tuymetova G, Harmon JM, Dunn TM, Proia RL. Autophagy regulates sphingolipid levels in the liver. *J Lipid Res* 2014; 55:2521-31; PMID:25332431; <http://dx.doi.org/10.1194/jlr.M051862>
- [57] Nixon RA, Yang DS. Autophagy failure in Alzheimer disease-locating the primary defect. *Neurobiol Dis* 2011; 43:38-45; PMID:21296668; <http://dx.doi.org/10.1016/j.nbd.2011.01.021>
- [58] Nixon RA. The role of autophagy in neurodegenerative disease. *Nat Med* 2013; 19:983-97; PMID:23921753; <http://dx.doi.org/10.1038/nm.3232>
- [59] Lee JK, Jin HK, Park MH, Kim B, Lee PH, Nakauchi H, Carter JE, He X, Schuchman EH, Bae J. Acid sphingomyelinase modulates the autophagic process by controlling lysosomal biogenesis in Alzheimer disease. *J Exp Med* 2014; 211:1551-70; PMID:25049335; <http://dx.doi.org/10.1084/jem.20132451>
- [60] Sgarbi G, Matarrese P, Pinti M, Lanzarini C, Ascione B, Gibellini L, Dika E, Patrizi A, Tommasino C, Capri M, et al. Mitochondria hyperfusion and elevated autophagic activity are key mechanisms for cellular bioenergetic preservation in centenarians. *Aging (Albany NY)* 2014; 6:296-31; PMID:24799450; <http://dx.doi.org/10.18632/aging.100654>
- [61] Mizushima N, Yoshimori T, Levine B. Methods in mammalian autophagy research. *Cell* 2010; 140:313-26; PMID:20144757; <http://dx.doi.org/10.1016/j.cell.2010.01.028>
- [62] Riemann D, Tcherkes A, Hansen GH, Wulfaenger J, Blosz T, Danielson EM. Functional co-localization of monocytic aminopeptidase N/CD13 with the Fc gamma receptors CD32 and CD64. *Biochem Biophys Res Commun* 2005; 331:1408-12; PMID:15883031; <http://dx.doi.org/10.1016/j.bbrc.2005.04.061>
- [63] Zamzami N, Maise C, Métévier D, Kroemer G. Measurement of membrane permeability and permeability transition of mitochondria. *Methods Cell Biol* 2001; 65:147-58; PMID:11381591; [http://dx.doi.org/10.1016/S0091-679X\(01\)65009-X](http://dx.doi.org/10.1016/S0091-679X(01)65009-X)
- [64] Wieckowski MR, Giorgi C, Lebiedzinska M, Duszynski J, Pinton P. Isolation of mitochondria-associated membranes and mitochondria from animal tissue and cells. *Protocol* 2009; 4:1582-90; <http://dx.doi.org/10.1038/nprot.2009.151>